Modulation of Rac1/PAK1/connexin43-Mediated ATP Release from Astrocytes Contributes to Retinal Ganglion Cell Survival in Experimental Glaucoma

Guo-Li Zhao
Fudan University Institutes of Brain Science
Hong Zhou
Fudan University Institutes of Brain Science
Shu-Min Zhong
Fudan University Institutes of Brain Science
Han Zhou
Fudan University Institutes of Brain Science
Lin-Jie Xu
Fudan University Institutes of Brain Science
Fang Li
Fudan University Institutes of Brain Science
Bo Lei
Henan Provincial People's Hospital
Zhongfeng Wang
Fudan University Institutes of Brain Science
Yanying Miao (yymiao@fudan.edu.cn)
Fudan University Institutes of Brain Science https://orcid.org/0000-0003-3948-2943

Research article

Keywords: glaucoma, Rac1, astrocyte, connexin43, ATP, retina

Posted Date: August 6th, 2021

DOI: https://doi.org/10.21203/rs.3.rs-770147/v1

Abstract

Background: Connexin43 (Cx43) is one of major gap junction proteins in glial cells. Mutation in the gap junction protein alpha 1 gene of Cx43 has been detected in human glaucomatous retinas, suggestive of involvement of Cx43 in pathogenesis of glaucoma. However, the role of Cx43 in glaucoma has not been clearly elucidated.

Methods: A mouse model of chronic ocular hypertension (COH) was produced by injecting magnetic microbeads into the eye anterior chamber. To explore the role of Rac1 in regulating Cx43 function, Rac1 conditional knockout in astrocytes was generated by subretinal injection of AAV-GFAP-Cre in $Rac1^{flox/flox}$ mice. The hemichannel activity was assayed by ethidium bromide uptake. The level and source of ATP were assayed by a commercial ATP assay kit, ATP sensors and removing microglia.

Results: In this study, we showed that Cx43 were mainly expressed in retinal astrocytes. Intraocular pressure (IOP) elevation induced astrocyte activation, as evidenced by increased expressions of c-Fos and glial fibrillary acidic protein (GFAP), which results in downregulation of Cx43 and changes of Cx43 phosphorylation at Ser373 and Ser368 sites. In the optic nerve head of COH mice, Cx43 expression in Gap43 (an activity-dependent plasticity protein) positive astrocytes was reduced. In COH retinas, Rac1, a member of the Rho family, was activated, which was consistent with the decrease of Cx43 expression in a time course. Pharmacological inhibition of Rac1 inhibited the activity of its downstream molecule PAK1, and reversed the reduction of Cx43 expression and astrocyte activation induced by IOP elevation. Co-immunoprecipitation experiments further demonstrated the interactions between Cx43 and active Rac1 or p-PAK1. Inhibition of Rac1 or conditional knockout of Rac1 in macroglial cells increased the ATP release through Cx43 hemichannels in astrocytes of COH retinas. Additionally, Rac1 deletion in astrocytes upregulated the expression of adenosine A3 receptor in retinal ganglion cells (RGCs) and promoted RGC survival, at least at early stage of IOP elevation through activating adenosine receptors.

Conclusions: Our results showed that Rac1 in astrocytes regulated glaucomatous RGC survival through Cx43-mediated ATP release. These findings suggest that modulation of Rac1/PAK1/Cx43 pathway in astrocytes may be a potential strategy of neuroprotection in glaucoma.

Introduction

Connexin43 (Cx43) is specialized in cell-to-cell connection that is an important part of maintaining the cell and tissue homeostasis. The mutation in the gap junction protein alpha 1 (GJA1) gene of Cx43 protein causes oculodentodigitaldysplasia (ODDD), which is accompanied with ocular disorders [1, 2], and this mutation is also detected in patients with open-angle glaucoma [3], suggesting that Cx43 may be involved in the pathogenesis of glaucoma.

Glaucoma is the leading cause of irreversible blindness diseases in the world, which is characterized by the optic nerve head (ONH) lesion and visual field loss. Retinal ganglion cell (RGC) apoptotic death is the fundamental pathological process of glaucoma. Intraocular hypertension is considered to be the most

important risk factor [4]. As one of the retinal neurodegenerative diseases, the pathogenesis of glaucoma is complex and diverse. Astrocytes, the major glia in the ONH [5], closely surround the non-myelinated sheath segment of RGC axons to provide energy to RGCs through morphological remodeling, in which Cx43 plays an important role.

In retina, Cx43 is the main gap junction protein in retinal glial cells including macroglia (Müller cells and astrocytes) and microglia [6, 7]. Connexon in one cell pairs with the same or a different type of connexons in neighboring cell to constitute gap junction, whereas in the membrane, connexin that does not find its matches forms a hemichannel. The hemichannels operate as a stand-alone gated pore [8, 9], opening to the extracellular space to release gliotransmitters, nicotinamide adenine dinucleotide or D-serine, and facilitate purinergic signaling. In retinal astrocytes, Cx43-mediated metabolic network serves as an endogenous mechanism to mitigate the bioenergetic stress and disperse the impact of neurodegenerative disease processes. Although Cx43 has been implicated in the pathological process of glaucoma, an exact association between Cx43 and RGC loss has not been completely elucidated. Previous studies have shown that partial superior optic nerve transection induced a biphasic up-regulation of retinal Cx43 proteins in the superior retina of rats, and RGC loss was associated with astrocyte-mediated inflammatory response [7]. In glaucomatous retina, intraocular pressure (IOP) elevation may induce the loss of gap junction communication and redistribution of Cx43 in astrocytes, thus changing the homeostasis of RGC axons and causing glaucomatous neuropathy [10]. In addition, blocking the Cx43 hemichannels reduced RGC apoptosis in glaucoma [11], indicating that modulating Cx43 hemichannels may provide neuroprotective effects in glaucoma.

Rac1 is an important member of the Rho GTPase of small G protein family. It controls cytoskeleton rearrangement, which causes structural changes in cell junctions. Rac1-mediated signaling, such as N-cadherin, MENA, or PAK1, modulates the expression and localization of Cx43 [12–15]. Our previous study has shown that Rac1 was activated in retinas of a mice experimental glaucoma model and regulated RGC autophagy and apoptosis [16]. In this study, we explored whether and how Rac1 may regulate Cx43 in retinal astrocytes and how Rac1 is involved in the astrocyte-RGC cross-talk in a mouse model of experimental glaucoma.

Materials And Methods

Animals

All procedures of animal experiments were carried out according to the National Institutes of Health (NIH) guidelines for the Care and Use of Laboratory Animals and approved by Fudan University Animal Care Committee. All efforts were made to minimize the animal's pain and discomfort during the experiments. C57BL/6 mice were purchased from the SLAC Laboratory Animal Co. Ltd (Shanghai, China). $Rac1^{flox/flox}$ mice were obtained from The Jackson Laboratory (Bar Harbor, ME, USA) [17]. hGFAP-cre mice were a generous gift from Dr. Lan Xiao (Army Medical University, Chongqing, China). Mice were housed in a cycle of 12 hours light/darkness with normal rodent food and water ad libitum.

COH mouse model

COH mouse model was produced according to our previous work [16]. In brief, the mice were anesthetized by intraperitoneal injection of 2% pentobarbital sodium (40 mg/kg), and then oxybuprocaine hydrochloride eye drops (4 mg/ml) were applied to the inner edge of the eyelid for topical anesthesia. Tropicamide eye drops (5 mg/ml) was used to dilate the pupils. Under the aid of the ophthalmic surgical microscope (OPMI VISU 140, Carl Zeiss, Jena, Germany), magnetic microbeads (diameter ≈ 9μm BioMag ® Superparamagnetic Iron Oxide, Bangs Laboratories, Ins, USA) (2 μl) were injected into the anterior chamber avoiding iris and lens injuries. The beads were evenly distributed around the iridocorneal angle by a handheld magnet (0.45 Tesla). In sham-operated groups (control), similar procedures were performed except for injecting 2 μl normal saline (NS). Chlortetracycline ointment was smeared on surface of the eye ball to prevent infection after operation. IOP was measured by a hand-held Tonolab rebound tonometer (Icare, Finland) at 9–10 a.m. to avoid possible circadian rhythm differences. IOPs of both eyes were recorded immediately after surgery (G0d), at the day 4 after surgery (G4d), and at the 1st, 2nd, 3rd, and 4th week after surgery (G1w, G2w, G3w and G4w, respectively). The average value of five consecutive acceptable measurements with a deviation 5% was recorded.

Western blotting analyses

Western blotting analyses were performed as described previously [18–20]. For whole cell protein extraction, retinas were homogenized in the RIPA lysis buffer supplemented with a mixture of protease and phosphatase inhibitors (Roche Applied Science, Mannheim, Germany). The extraction of retinal plasma membrane protein was followed the instructions of a commercial plasma membrane protein extraction kit (Bio Vision, Milpitas, CA, USA). The protein concentrations were determined by standard bicinchoninic acid assay kit (Pierce Biotechnology, Rockford, IL, USA). According to the molecular weights of the target proteins, the protein samples were separated by 8%, 10% or 15% of twelve alkyl sulphate polyacrylamide gel electrophoresis (SDS-PAGE) respectively, and then transferred from the gels onto PVDF membranes (Immobilon-P, Millipore, Billerica, MA, USA) using Mini-PROTEAN 3 Electrophoresis System and Mini Trans-Blot Electrophoretic Transfer System (Bio-Rad, Hercules, CA, USA). The antibodies used in this study were listed in the Supplementary Table 1. Digital imager (FluorChem E System, ProteinSimple, San Jose, CA, USA) was used for imaging, and AlphaView SA (version 3.4, ProteinSimple) was used for analysis.

Co-immunoprecipitation

Co-immunoprecipitation (Co-IP) experiments were conducted to test possible interactions of Cx43 and active Rac1 or p-PAK1. The procedure was performed according to the Pierce Co-IP kit instructions (Pierce™, Thermo -Fisher Scientific, Pittsburgh, PA, USA) [16]. The Cx43 antibody was purified with a Pierce Antibody Clean-up Kit (Thermo -Fisher Scientific). Retinal protein extracts were obtained from control (Ctr) and COH retinas of G1w. Subsequent procedure was performed, similar to Western blotting.

Immunofluorescent staining

Immunohistochemistry was performed as previously described [18–20]. Briefly, the eye cup was fixed with 4% paraformaldehyde in 0.1 M phosphate-buffered saline (PBS) (pH 7.4) for 4 h at room temperature. After dehydration and embedding of retinas in OCT compound (Tissue Tek, Torrance, CA), the retinal sections with a thickness of 14 μm were cut vertically on a frozen microtome (Leica, Nussloch, Germany). At room temperature, 5% normal donkey serum and 1% BSA in PBS containing 0.1% Triton X-100 were used to block the sections or whole flat-mounted retinas for 2 h. The samples were incubated overnight (for retinal sections) or 3 days (for whole flat-mounted retinas) at 4°C with the primary antibodies, and then with the second antibodies listed in Supplementary Table 1. Then the samples were mounted with anti-fade mounting medium with DAPI (Vector Laboratories, Burlingame, CA, USA), and images were captured with FV1000 confocal laser-scanning microscope (Olympus, Tokyo, Japan). In order to avoid any possible reconstruction stack artifacts, a single-layer optical slice was scanned at 1.0 μm intervals to accurately evaluate the double markers.

Measurement of ATP levels

Retinas were collected from eyes and adenosine triphosphate (ATP) levels were determined by luciferin-luciferase method according to the instructions of ATP Detection Kit (Beyotime Biotechnology Inc., Shanghai, China). In some experiments, the ecto-ATPase inhibitor ARL67156 (100 μM, Sigma-Aldrich, MO, USA) was added to the tissue lysate to prevent ATP degradation. ATP levels were calculated from an ATP standard curve which was prepared in concentration of 1 nM to 10 μM, and adjusted to protein concentration determined by BCA method (Pierce). The ATP levels were expressed as relative ratio to control.

EtBr uptake

After separated, retinas were immediately incubated in PBS containing 4 μM Ethidium Bromide (EtBr) (Sigma-Aldrich, MO, USA) for 10 min at room temperature [21, 22]. Then the retinas were processed for immunohistochemistry.

Intravitreal injection

Intravitreal injection was performed as our previous descriptions [19, 20, 23]. The pupil of the anaesthetized animal was dilated with topiramate eye drops. NSC23766 (500 μM, Tocris Bioscience, Bristol, UK), Gap26 (200 μM, ApexBio, Houston, USA), Gap19 (250 μM, Tocris Bioscience) or CGS 15943 (10 μM, Tocris Bioscience) dispersed in 2 μl 0.9% NS, were injected into the vitreous body of the eyes by using a 30-gauge Hamilton micro-injector (Hamilton, Reno, NV, USA) under a stereoscopic microscope (Carl Zeiss, Oberkochen, Germany). Same volume of NS was injected in the control mice.

Intraperitoneal injection of clodronate liposomes

Chlodronate liposomes (Clo-lip) (50 mg/ml) and control (PBS) liposomes (PBS-lip) (liposoma B.V., Amsterdam, The Netherlands) were intraperitoneally injected with 10 mg/kg. Seven days later, the retinas were collected for subsequent experiments.

Virus injection

GFAP-Cre-AAV and GFP-AAV (control) were purchased from OBiO Technology (Shanghai, China). The viruses were injected into the retina under Olympus ZS61 microscope (Olympus, Tokyo, Japan) using Nanoject II micro-injector (Drummond Scientific Company, Broomall, PA, USA) with a micropipette of 10–30 μm tip size, respectively. Rac1 conditional knockout in astrocytes was generated by sub-retinal injection of GFAP-Cre-AAV (2 μl, 1.36 $\times 10^{13}$ v.g./ml) in $Rac1^{flox/flox}$ mice. An equal volume of GFP-AAV (empty vector) was injected in $Rac1^{flox/flox}$ mice as controls. Three weeks later, the subsequent experiments were carried out.

Fluorescence imaging of ATP sensors

AAV2-EFS-DIO-ATP1.0 (Vigene Bioscience, Maryland, USA) is a genetically encoded G protein-coupled receptor (GPCR)-activation-based (GRAB) sensor for ATP (GRABAtp), in which the amount of extracellular ATP is indicated by the intensity of fluorescence produced by green fluorescent protein (GFP) [24]. The AAV viruses were injected into retinas of hGFAP-cre mice 3 weeks before the other operations. NS or NSC23766 was injected into the vitreous body one day before the COH operation. The retinas were collected at G1w and immediately incubated in pre-oxygenated artificial cerebral spinal fluid (ACSF) solution [17]. The area with fluorescent signals was selected for shooting as fast as possible to keep the retinal cells alive in the Nikon Live Cell Workstation (Nikon Corporation, Tokyo, Japan). Immunostaining images were analyzed by Image-Pro Plus software (Image-Pro Plus, RRID: https://scicrunch.org/resolver/SCR_007369, Media Cybernetics, Inc. USA). The average fluorescence intensity for a single cell was represented by IOD (Integrated Optical Density)/cell area.

Statistical analyses

All data in this study are presented as the mean ± SEM. GraphPad Prism (version 6.0; GraphPad Software, San Diego, CA, USA) was used to analyze the data. The differences between two groups were compared by two-tailed unpaired t-test. One-way ANOVA with Tukey's multiple comparison test was used to compare data from multiple groups. In all tests, *P* values of less than 0.05 were considered statistically significant.

Results

Cx43 is mainly expressed in astrocytes in mouse retina

We first examined the expression and distribution of Cx43 in mouse retina. Figure 1 shows that Cx43 was mainly distributed in the retinal nerve fiber layer (NFL). Double immunostaining further showed that Cx43 was not co-labeled with brain-specific homeobox/POU domain protein 3A (Brn3a), a marker of RGCs (Fig. 1A, a1-a3), but was predominantly co-labeled with glial fibrillary acidic protein (GFAP), a marker of astrocytes (Fig. 1B, b1-b3). A small amount of Cx43 was expressed in the end-feet of Müller cells, as shown the co-localization of Cx43 and glutamine synthase (GS, a marker of Müller cells) in the NFL (Fig. 1C, c1-c3), and in microglia labeled by ionized calcium binding adapter molecule 1 (Iba-1) in the inner plexiform layer (IPL) (Fig. 1D, d1-d3).

Up-regulation of Cx43 phosphorylation in COH retinas

Dynamic changes in the protein levels of total and phosphorylated Cx43 in COH retinas were then examined. The COH mouse model was successfully produced, with the IOPs in the operated eyes ranging from 14.9 ± 0.3 mmHg at G4d (n = 41, all $P < 0.001$) to 17.7 ± 0.4 mmHg at G4w (n = 28, all $P < 0.001$), which was significantly higher than that of 0d or the corresponding un-operated eyes (9.93 ± 0.02, n = 141), and the sham-operated eyes (9.91 ± 0.02, n = 150) (Fig. 2A).

The phosphorylation of Cx43 at Ser373 site (p-Cx43^{Ser373}) and at Ser368 site (p-Cx43^{Ser368}) are two important modulated ways, which may affect Cx43 hemichannel functions [25–29]. In our COH retinas, total protein levels of Cx43 were significantly decreased at G4d and G1w (n = 6, $P < 0.01$ and 0.001 *vs.* control (Ctr), respectively), then returned to the control levels at G2w and G3w, and decreased again at G4w (n = 6, $P < 0.01$ *vs.* Ctr) (Fig. 2B, C). The expression of p-Cx43^{Ser373} was significantly decreased at G1w (n = 6, $P < 0.05$ *vs.* Ctr) and then quickly returned to the control levels (Fig. 2B, D), while the levels of p-Cx43^{Ser368} did not show significant change as compared with Ctr at G4d and G1w, followed by significant decrease from G2w to G4w (n = 6, $P < 0.05$ and 0.01 *vs.* Ctr) (Fig. 2B, E). These changes resulted in a significant increase of the ratio of p-Cx43^{Ser373}/Cx43 (red dash line) at G4w ($P < 0.001$) (Fig. 2D) and an up-regulation of the ratio of p-Cx43^{Ser368}/Cx43 (red dash line) at G4d and G1w ($P < 0.01$ and 0.001, respectively) (Fig. 2E). Since Cx43 proteins only expressed on cell membrane could form functional hemichannels, we further detected the Cx43 protein levels in the membrane component. As shown in Fig. 2F-I, changes of Cx43, p-Cx43^{Ser373}, p-Cx43^{Ser368}, ratios of p-Cx43^{Ser373}/Cx43 and p-Cx43^{Ser368}/Cx43 in membrane proteins of COH retinas were basically consistent with those in total retinal proteins, suggesting that the functions of Cx43 hemichannels were modulated after IOP elevation.

Dynamic changes of Cx43 expression caused by astrocyte plasticity in the ONH of COH mice

In the ONH, astrocytes form functional syncytia through the gap junctions constructed by Cx43, thereby communicating with RGCs and maintaining the ion and metabolic homeostasis of RGCs [10]. To test whether astrocytes may be responded to the changes of Cx43 after IOP elevation, we examined the activation of astrocytes in COH retinas by c-Fos immunostaining, an immediate early gene. As shown in Fig. 3, weak c-Fos positive fluorescent signals were detected in the ONH of sham-operated retinas (control, Ctr) (Fig. 3A, a1), and more c-Fos positive signals appeared at G4d in COH mice and then the number of positive signals was progressively increased until G4w (Fig. 3Bb1, 3Cc1, 3Dd1, 3Ee1, and 3Ff1). The c-Fos positive signals were co-located with GFAP (Fig. 3Bb3, 3Cc3, 3Dd3, 3Ee3, and 3Ff3). In addition, the cells in the inner and outer nuclear layers (INL and ONL) began to be activated at G1w, and the c-Fos positive signals in RGCs were seen from G2w (Fig. 3D-3F, arrows). These results suggest the astrocyte activation was prior to neurons in COH retinas. The increased protein levels of GFAP indicate that macroglial cells were activated after IOP elevation in COH retinas (n = 6, $P < 0.05 \sim 0.001$ *vs.* Ctr) (Fig. 3G, H).

Then, we detected the astrocyte plasticity in the ONH after IOP elevation. Growth-associated protein 43 (Gap43), an activity-dependent plasticity protein [30], is implicated in axonal plasticity and regeneration [31]. We first identified the glial cell types that express Gap43 in the ONH. Our results showed that Gap43 was mainly expressed in astrocytes labeled by GFAP (Fig. 4A), scarce in Müller cells labeled by GS (Fig. 4B), less in oligodendrocytes labeled by O4 (Fig. 4C) and microglia labeled by Iba-1 (Fig. 4D). We then detected the expression of Cx43 in the Gap43 positive cells by double immunostaining (Fig. 4E). Although the number of Gap43 labeled cells kept unchanged during the whole period of IOP elevation (G4d-G4w) (n = 5 ~ 6, $P > 0.05$ *vs*. Ctr) as compared with the controls (Fig. 4E, F), the fluorescent intensity of Gap43 was increased in COH retinas (Fig. 4E, e8-e12). The number of Gap43 and Cx43 double labeled cells was significantly decreased from G4d to G2w in COH retinas (n = 5 ~ 7, $P < 0.05$ and 0.01 *vs*. Ctr), and then returned to the control levels (Fig. 4E, G). Similarly, Western blotting experiments showed that the protein levels of Cx43 in the ONH were decreased from G4d to G2w (n = 5, $P < 0.01$ *vs*. Ctr) (Fig. 4H, I). These results suggest that the plasticity of astrocytes in the ONH may cause the reduced expression of Cx43 during IOP elevation.

Rac1 regulates astrocyte response in COH retinas

The regulation of cytoskeleton and differentiation is involved in the plasticity of astrocytes. Previous studies have shown that Rac1, a GTPase of the Rho family, was specialized in the regulation of actin cytoskeleton dynamics [32, 33], which was involved in the pathogenesis of glaucoma. We examined whether Rac1 may be involved in the regulation of astrocyte activation in COH retina. As shown in Fig. 5A and 5B, the ratio of active Rac1 to Rac1 in COH retina was significantly increased at G4d and G3w (n = 6, $P < 0.01$ and 0.001 *vs*. Ctr, respectively), similar to our previous report [16]. Additionally, the expression of GFAP was increased in COH retina (normal saline (NS) G1w) (n = 6, $P < 0.001$ *vs*. Ctr), which could be largely reversed by NSC23766 (NSC) administration, an inhibitor of Rac1 (n = 6, $P < 0.001$ *vs*. Ctr and NS G1w) (Fig. 5C, D). IOP elevation in COH retina induced morphological changes of astrocyte from the smaller cell bodies with slender processes in control condition to the larger cell bodies with more branches and hypertrophic protrusion. These morphological changes of astrocytes could be partially reversed by the Rac1 inhibitor NSC23766 (n = 5, $P < 0.001$ *vs*. Ctr, $P < 0.01$ *vs*. NS G1w group) (Fig. 5E, F). Furthermore, inhibition of Rac1 by NSC23766 significantly increased the EtBr uptake of astrocytes in COH retinas (n = 6, $P < 0.01$ *vs*. NS G1w group), suggesting that Rac1 regulates the permeation of hemichannels in astrocytes. The increased permeation mediated by Rac1 inhibition was blocked by the Cx43 inhibitor Gap26 (n = 6, $P < 0.05$ *vs*. NSC G1w group), further demonstrating that it was the hemichannels mediated the EtBr uptake in astrocytes (Fig. 5G, H).

The above results show that changes in expression of Rac1 in COH retinas are opposite to those of Cx43. It is possible that Rac1 may regulate the expression of Cx43. To test this possibility, the Rac1 inhibitor NSC23766 was intravitreally injected 2 days prior to the operation of COH model. As shown in Fig. 6A and 6B, the total protein levels of Cx43 were significantly increased in COH retinas when Rac1 was inhibited (n = 6, $P < 0.001$ *vs*. NS G1w). At the same time, the expression of p-Cx43^{Ser373} was increased (Fig. 6A and

6C), while the expression of p-Cx43^{Ser368} was decreased (n = 5, *P* all < 0.05 *vs*. NS G1w) (Fig. 6A and 6D). Furthermore, the protein levels of Cx43 in membrane component were also significantly increased (n = 7, *P* < 0.001 *vs*. NS G1w). PAK1 is a downstream molecule of Rac1. Pre-injection of the Rac1 inhibitor NSC23766 significantly reduced the protein levels of active Rac1 and p-PAK1 in COH retinas, which resulted in decreased ratios of active Rac1/Rac1 and p-PAK1/PAK1 (n = 6, *P* < 0.01 and 0.05, respectively) (Fig. S1, A-C). In addition, pre-injection of the PAK1 inhibitor IPA-3 (4 mg/kg, i.p.) significantly reduced the protein levels of PAK1 and p-PAK1 in COH retinas (n = 6, *P* all < 0.001 *vs*. NS G1w) (Fig. S1, D-G). Moreover, although pre-injection of IPA-3 did not affect the protein levels of Cx43, the protein levels of p-Cx43^{Ser373} were up-regulated (n = 5, *P* < 0.001 *vs*. NS G1w) and the protein levels of p-Cx43^{Ser368} were down-regulated (n = 6, *P* < 0.01 *vs*. NS G1w), similar to that of the Rac1 inhibition (Fig. 6G-J). Co-IP experiments further revealed that there were interactions between Cx43 and active Rac1 or p-PAK1 (Fig. 6K, L). These results suggest that Rac1/PAK1 signaling pathway may directly regulate the phosphorylation of Cx43.

Rac1-mediated ATP release from astrocytes

In COH retinas, extracellular ATP concentrations were progressively increased from G2w to G4w (n = 5∼7, *P* < 0.05∼0.001 *vs*. Ctr) (Fig. 7A). However, when the ecto-ATPase inhibitor ARL67156 was added to the tissue lysate to prevent ATP degradation, a significant increase of ATP concentration was also observed at G4d and G1w (n = 6, *P* all < 0.01 *vs*. Ctr) (Fig. 7B), suggestive of a quick degradation of ATP at early stage of IOP elevation. Furthermore, inhibiting the activation of Rac1 by NSC23766 promoted the release of ATP at G1w and G2w (n = 6, *P* all < 0.01 *vs*. NS groups) (Fig. 7C, D), while inhibition of Cx43 by Gap26 or Gap19 significantly reduced the ATP levels (n = 6, *P* < 0.05 and 0.01, respectively) (Fig. 7C, D), suggesting that Rac1 regulates ATP release in COH retinas through affecting Cx43 hemichannels. Cx43 is expressed on astrocytes, Müller cells and microglia. In order to determine whether inhibition of Rac1 increase ATP release from microglia, a single dose of clodronate liposomes (Clo-lip) was intraperitoneally injected one day before the COH operation to remove microglia. Clo-lip treatment could remove about 66.1 ± 2.9 % of microglia in retina (Fig. S2). Figure 7E shows that removing retinal microglia did not affect the increased ATP levels caused by the Rac1 inhibitor NSC23766 in COH retinas, indicating that microglia was not the source of Rac1-mediated ATP release (Fig. 7E). In order to identify whether ATP may be released from astrocytes, the AAV2-EFS-DIO-ATP1.0 probe was injected into the retinas of GFAP-Cre mice to make the ATP probe express specifically in astrocytes (Fig. 7F). Three weeks after the AAV injection, NSC23766 was intravitreally injected before the COH operation. The fluorescent signals of GFP were detected in the living retina at G1w. We observed that the Rac1 inhibitor NSC23766 significantly increased the fluorescent signal density (n = 45 cells of 3 retinas, *P* < 0.001), as compared with the controls (NS) (n = 43 cells of 3 retinas) (Fig. 7G, H). These results indicate that GFAP-positive astrocytes contribute to the increased extracellular ATP concentrations.

We then explored whether conditional knockout of Rac1 in astrocytes may affect Cx43-mediated ATP release. Rac1 knockout in astrocytes was constructed by intravitreally injecting GFAP-Cre-AAV into

Rac1$^{flox/flox}$ mice. The efficiency of Rac1 knockout in astrocytes was shown in Fig. S3. Compared with GFP-AAV-injected group, the number of GFAP and Rac1 co-localized positive signals was reduced in GFAP-Cre-AAV injected group (Fig. S3). The protein levels of Cx43 were increased in COH retinas at G1w in the Rac1 conditional knockout mice (n = 6, $P < 0.01$ *vs*. GFP-AAV group) (Fig. 7I, J), and the ATP concentrations were also increased in COH retinas of the Rac1 conditional knockout mice (Fig. 7K).

Rac1-mediated ATP release increases the survival of RGCs in COH retinas

What's the role of the Rac1-mediated ATP release from astrocytes on RGC survival in glaucoma? We assayed the survival of RGCs by Brn3a immunostaining in whole flat-mounted retinas. Figure 8A shows representative images obtained from central and peripheral areas of retinas at the same angle (Fig. 8B). The average number of RGCs in both the central and peripheral areas of COH retinas at G1w was significantly increased in the Rac1 conditional knockout mice (n = 5, $P < 0.001$ and 0.01 *vs*. GFP AAV group, respectively), which could be blocked by Gap26 administration (n = 6, $P < 0.001$ and 0.05 *vs*. GFAP Cre AAV group, respectively) (Fig. 8C). These results suggest that conditional knockout of Rac1 in astrocytes may increase RGC survival through modulating Cx43.

We then explored how conditional knockout of Rac1 in astrocytes protects RGCs in COH retina. As shown in Fig. 8D, adenosine A1 receptor (A1R) and A3 receptor (A3R) were expressed in Brn3a-positive RGCs. IOP elevation did not change the expression of A1R (d2) and A3R (d5). Similar results were observed when Rac1 was inhibited by the NSC23766 injection in COH retinas (Fig. 8D, d3). However, injection of NSC23766 remarkably augmented the expression of A3R in Brn3a-positive RGCs in COH retinas (Fig. 8D, d6), which was further confirmed in conditional knockout of Rac1 in astrocytes (Fig. 8E). Furthermore, in the Rac1 conditional knockout mice, intravitreal injection of CGS 15943, an adenosine receptor antagonist, partially attenuated the increase in the number of Brn3a positive RGCs in both central and peripheral areas of COH retinas (n = 6, $P < 0.01$ and 0.001 *vs*. GFAP AAV Cre groups, respectively) (Fig. 8F-H). All these results suggest that Rac1-mediated ATP release increases the survival of RGCs through activating adenosine receptors.

Discussion

Dynamic changes of Cx43 hemichannels in astrocytes of COH retinas

Cx43 is the most widely studied gap-junction forming protein in the central nervous system (CNS), which is specifically expressed in astrocytes. Previous studies have shown that Cx43 was expressed in retinal Müller cells [6] and microglia [34]. In this study, we clearly showed that Cx43 proteins were expressed and distributed in the cells of the NFL and GCL, which were mainly co-localized with the astrocyte marker GFAP and sparsely presented in the end-foot of Müller cells and microglia (Fig. 1). In COH retinas, the expression of Cx43 showed biphasic down-regulation (at G4d to G1w, and G4w) (Fig. 2). Indeed, dynamic

changes in Cx43 expression were observed in various diseases. For example, the increased expression of Cx43 was observed in cerebral hypoxic preconditioning, hippocampal seizures, and human epileptic and drug-resistant cerebral cortex [35–37]. Down-regulation of Cx43 was also reported in heart failure [38, 39] and cerebral ischemia/reperfusion [40]. The different expression pattern of Cx43 may be due to tissue specificity and different pathological process [41].

The detailed mechanisms underlying downregulation of Cx43 in glaucomatous retina are not clear. We speculate that the changes of Cx43 may be associated with the plastic changes of astrocytes during IOP elevation. Firstly, in response to IOP elevation, astrocytes were activated and underwent morphologic and functional changes (Fig. 3). Gap43 protein is a marker of activity-dependent plasticity in astrocytes [30]. The immunofluorescent densities of Gap43 in astrocytes of COH retinas were significantly increased (Fig. 4E), indicating an increased activity of astrocytes. In Gap43-positive astrocytes, the expression of Cx43 was reduced (Fig. 4E, G). Secondly, during plastic changes in response to IOP elevation, astrocytes underwent structural remodeling and Cx43 may be re-distributed, which may require, at least, transient breakdown of Cx43 gap junctions [42]. Thirdly, the degradation of Cx43 in glaucoma may be accelerated. In response to the elevated pressure, epidermal growth factor receptor (EGFR) was activated, leading to decrease of gap junction intercellular communication (GJIC) via tyrosine phosphorylation of Cx43 in ONH astrocytes [10], and inducing the binding of ubiquitin and target Cx43 to increase the internalization and degradation of Cx43 in a proteasome-dependent manner [43]. It was reported that epidermal growth factor (EGF) indeed induced a down-regulation of Cx43 expression in cultured rat cortical astrocytes [44].

The phosphorylation of Cx43 is crucial to regulate the function of gap junctions, trafficking and assembly of connexins [45]. Phosphorylation of Cx43 at S368 results in Cx43 internalization and down-regulation of GJIC [43], while phosphorylation at S373 induces an acute increase in gap junction size [46] and an enhancement of channel formation [47]. In this study, we showed that p-Cx43^{S368}/Cx43 was elevated at the early stage, and p-Cx43^{S373}/Cx43 was significantly increased at late stage both in total and membrane component of retinal proteins in COH retinas, suggesting that in response to IOP elevation, Cx43 hemichannels in astrocytes may be modulated, thus affecting the function of Cx43. In addition, inhibition of PAK1 increased the levels of p-Cx43^{S373} and decreased the levels of p-Cx43^{S368} in COH retinas (Fig. 6G-J). It was reported that the levels of p-Cx43^{Ser373} may indicate the open of the channel and the levels of p-Cx43^{Ser368} may present the close of channel [25–29]. The Rac1/PAK1 mediated changes in phosphorylated states of Cx43 may increase ATP release from astrocytes at early stage of IOP elevation. It should be noted that the relative levels of p-Cx43^{Ser368} were increased at G4d and G1w in COH retinas (Fig. 2E), however, extracellular ATP concentrations were still increased (Fig. 7B). We speculate that in case of onset of IOP elevation, mechanical pressure triggered ATP release from astrocytes is not in a linear manner with Cx43 expression since Cx43 may undergo a rearrangement. Inhibition of Rac1 could remodel the state of astrocytes and maintain the syncytial body of astrocytes in a state of coordinated response, which provides mechanical stability to against pressure [48]. At this time, the state of Cx43 hemichannels is linearly regulated for ATP release. The detained mechanisms remain to be explored in the future studies.

Rac1 modulates ATP release from astrocytes through Cx43 in COH retinas

Increasing evidence shows the importance of the Rho family in gap junction formation [12–15]. We showed that IOP elevation induced a biphasic upregulation in Rac1 activity, as evidenced by increased ratio of active Rac1/Rac1 (Fig. 5). It should be noted that the increase of Rac1 activity was consistent with the decrease of Cx43 expression in time course. We provide robust evidence demonstrating that changes in Cx43 expression of astrocytes in COH retina was caused by Rac1 activation. Inhibition of Rac1 or deletion of Rac1 in astrocytes negatively regulated the expression and function of Cx43 (Figs. 5 and 6). Inhibition of the Rac1 downstream molecule PAK1 reversed the IOP elevation induced changes in p-Cx43^{Ser368} and p-Cx43^{Ser373} in COH retinas, resulting in Cx43 hemichannels in an open state. Co-IP experiments demonstrated the interactions of Rac1/PAK1 with Cx43 (Fig. 6). Indeed, the interaction of PAK1 and Cx43 was found in cardiac myocytes, and activated PAK1 may dephosphorylate Rac1 in a negative feedback manner [49], and selectively released Rac1 from the TrkB.T1-associated RhoGDI by binding and phosphorylating RhoGDI [50]. Constitutive activated Rac1 may result in redistribution of Cx43 [14]. As a signal transduction hub, Rac1 may mediates N-cadherin signals that regulated the localization of Cx43 in aligned cardiac myocytes [12]. The interaction of Cx43 and Rac1 could be regulated by Mena, a member of the Ena/VASP family [14]. Additionally, it was reported that Rac1 can be activated by cAMP/PKA signaling [51–53], and elevated intracellular cAMP could increase Cx43 phosphorylation [54] and gap junction assembly [55]. In DBA/2J spontaneous glaucoma mice, cAMP immunoreactivities in retinal astrocytes was increased, which may exacerbate astrocyte vulnerability to oxidative stress [56]. Therefore, Rac1 may regulate the function of Cx43 in both direct and indirect pathways in glaucoma.

Our results showed that the levels of extracellular ATP were increased in glaucomatous retinas (Fig. 7). The sources of extracellular ATP may be from retinal neurons and glial cells since it was reported that mechanical pressure can trigger the release of ATP from these cells [57]. In this study, we provide evidence showing that Cx43-mediated ATP release in astrocytes of COH retina may be a main pathway. Inhibiting Rac1 or conditional knockout of Rac1 in astrocytes increased ATP concentrations in COH retinas, which could be blocked by the Cx43 inhibitors Gap26 and Gap19 (Fig. 7). However, partial depletion of microglia had no significant affection on ATP release, excluding microglia-mediated ATP release. It should be noted that Cx43 was also expressed in the endfeet of Müller cells (Fig. 1), and conditional knockout of Rac1 in the GFAP-cre mice may also delete Cx43 expressed in Müller cells. In the NFL, although the changes in ATP fluorescence signals acquired by ATP probe were mainly from astrocytes (Fig. 7F), we cannot exclude ATP release from Müller cells, which remains to be studied in the future. On the other hand, metabolic response after trauma can avoid energy deficiency of RGCs. In order to alleviate the energy barrier of RGCs, excessive ATP is produced by abnormal mitochondrial oxidative phosphorylation. At the same time, the overload of oxidative phosphorylation produces a large amount of ROS, which is not conducive to the survival of RGCs [58]. When the intracellular ATP concentration is increased, the state of Cx43 hemichannels has been usually adjusted to adapt the release of ATP. In

addition, Rac1 also regulates the key enzymes of glycolysis and oxidative phosphorylation to affect the release of ATP [59, 60].

Rac1/Cx43/ATP/A3R signaling-mediated the cross-talk between astrocytes and RGCs in COH retinas

ATP exerts its functions through two pathways, directly stimulating purinergic receptors and indirectly stimulating adenosine receptors after being converted to adenosine by extracellular ectonucleotidases (ecto-ATPase) [61, 62]. There is evidence demonstrating that ATP can induce retinal neuronal death by activating P2X7 receptor (P2X7R) [63]. In contrast, adenosine could provide neuroprotective by stimulating adenosine A1R and A3R [64, 65]. Therefore, the net effect of increased extracellular ATP on RGC survival in COH retina depend on the balance of ATP and adenosine [63]. In this study, we showed that in the presence of ecto-ATPase inhibitor ARL 67156, IOP elevation induced an increase in extracellular ATP levels and Rac1 deletion in astrocyte further promoted the increase. However, under the conditions of without the presence of ARL 67156, ATP concentrations only showed an increase tendency at the early stage of IOP elevation (G4d and G1w), suggesting that ATP may be rapidly degraded to adenosine. At the same time, adenosine A3R expression in RGCs was increased. These factors may together contribute to increased RGC survival in COH retina, at least in the early stage of glaucoma. Inhibition of Rac1 or Rac1 deletion in astrocyte increased the expression of Cx43 and ATP release, which may further increase adenosine, thus providing neuroprotective effect (Fig. 8). It is noteworthy that progressive IOP elevation induced higher levels of ATP (Fig. 7A), which may contribute RGC damage by stimulating P2X7R [63, 66, 67].

Additionally, the effects of astrocytes on retinal neurons may also depend on the functional states of astrocytes. Acute stress changes the structure and function of astrocytes, such as inducing cell hypertrophy, and reducing the gap junction coupling between cells, which result in the individual astrocytes separating themselves from the network, thus reducing their ability to supply energy for neurons [68]. Inhibition of Rac1 or conditional knockout of Rac1 increased the expression of Cx43, remodeled astrocytes and reduced the reactivity of astrocytes. Cx43-mediated astrocyte metabolic network as an endogenous mechanism can alleviate the bio-energy stress in the stress response [69].

In conclusion, our results provide robust evidence demonstrating that Cx43 are mainly expressed in retinal astrocytes. IOP elevation in mouse COH model induces astrocyte activation, which results in decreased expression of Cx43 and upregulated levels of p-Cx43. Conditional knockout Rac1 in astrocytes enhances ATP release through Cx43 hemichannels, which promotes RGC survival at early stage of glaucoma through modulating adenosine receptors. These results, together with our previous report [16], suggest that modulation of Rac1 may be a potential strategy of neuroprotection in glaucoma.

Abbreviations

A1R, A1 receptor

A3R, A3 receptor

ACSF, artificial cerebral spinal fluid

ATP, adenosine triphosphate

Brn3a, brain-specific homeobox/POU domain protein 3A

Clo-lip, clodronate liposomes

CNS, central nervous system

COH, chronic ocular hypertension

Co-IP, co-immunoprecipitation

Ctr, control

Cx43, connexin43

EGF, epidermal growth factor

EGFR, growth factor receptor

EtBr, ethidium Bromide

Gap43, growth-associated protein 43

GCL, ganglion cell layer

GFAP, glial fibrillary acidic protein

GFP, green fluorescent protein

GJA1, gap junction protein alpha 1

GJIC, gap junctional intercellular communication

GS, glutamine synthase

Iba1, ionized calcium binding adapter molecule 1

IOD, integrated optical density

IOP, intraocular pressure

IPL, inner plexiform layer

NFL, retinal nerve fiber layer

NS, normal saline

ONH, optic nerve head

ONL, outer nuclear layers

P2X7R, P2X7 receptor

PBS, phosphate-buffered saline

PBS-lip, PBS liposomes

RGCs, retinal ganglion cells

RNFL, retinal nerve fiber layer

Declarations

Ethics approval and consent to participate

All experimental procedures described in this article were approved by the animal care committee of Institutes of Brain Science at Fudan University.

Consent for publication

All authors have approved the contents of this manuscript and approved consent for publication.

Availability of data and materials

The data supporting the findings of this study are available within this article and its Supplemental Information Files. All other relevant data are available from the corresponding authors upon reasonable request. Source data are provided with this paper.

Competing interests

The authors declare no competing interests.

Finding

This work was supported by grants from the National Natural Science Foundation of China (81790642, 31872765), the Shanghai Municipal Science and Technology Major Project (No.2018SHZDZX01), ZJ Lab, and Shanghai Center for Brain Science and Brain-Inspired Technology.

Author contributions

Conception and design: Z.W., and Y.M.; performed the research and data collection: G.L.Z, H.Z., S.M.Z., H.Z., and L.J.X.; data analysis and interpretation: G.L.Z, B.L., Z.W., and Y.M.; drafted the manuscript: G.L.Z, Z.W., and Y.M.

Acknowledgments

We thanks Dr. Xiong-Li Yang for helpful discussion and critical comments on the manuscript.

References

1. Laird DW. Syndromic and non-syndromic disease-linked Cx43 mutations. FEBS Lett. 2014;588(8):1339–48. https://doi.org/j.febslet.2013.12.022.
2. Wang Z, Sun L, Wang P, Chen C, Zhang A, Wang W, et al. Novel ocular findings in oculodentodigital dysplasia (ODDD): a case report and literature review. Ophthalmic Genet. 2019;40(1):54–9. https://doi.org/10.1080/13816810.2019.1571616.
3. Huang X, Wang N, Xiao X, Li S, Zhang Q. A novel truncation mutation in GJA1 associated with open angle glaucoma and microcornea in a large Chinese family. Eye (Lond). 2015;29(7):972–7. https://doi.org/10.1038/eye.2015.74.
4. Frankfort BJ, Khan AK, Tse DY, Chung I, Pang JJ, Yang Z, et al. Elevated intraocular pressure causes inner retinal dysfunction before cell loss in a mouse model of experimental glaucoma. Invest Ophthalmol Vis Sci. 2013;54(1):762–70. https://doi.org/10.1167/iovs.12-10581.
5. Lozano DC, Choe TE, Cepurna WO, Morrison JC, Johnson EC. Early optic nerve head glial proliferation and Jak-Stat pathway activation in chronic experimental glaucoma. Invest Ophthalmol Vis Sci. 2019;60(4):921–32. https://doi.org/10.1167/iovs.18-25700.
6. Zahs KR, Kofuji P, Meier C, Dermietzel R. Connexin immunoreactivity in glial cells of the rat retina. J Comp Neurol. 2003;455(4):531–46. https://doi.org/10.1002/cne.10524.
7. Chew SSL, Johnson CS, Green CR, Danesh-Meyer HV. Response of retinal connexin43 to optic nerve injury. Invest Ophthalmol Vis Sci. 2011;52(6):3620–9. https://doi.org/10.1167/iovs.10-6318.
8. Caspar DL, Goodenough DA, Makowski L, Phillips WC. Gap junction structures. I. Correlated electron microscopy and x-ray diffraction. J Cell Biol. 1977;74(2):605–28. https://doi.org/10.1083/jcb.74.2.605.
9. Falk MM, Buehler LK, Kumar NM, Gilula NB. Cell-free synthesis and assembly of connexins into functional gap junction membrane channels. EMBO J. 1997;16(10):2703–16. https://doi.org/10.1093/emboj/16.10.2703.
10. Malone P, Miao H, Parker A, Juarez S, Hernandez MR. Pressure induces loss of gap junction communication and redistribution of connexin 43 in astrocytes. Glia. 2007;55(10):1085–98. https://doi.org/10.1002/glia.20527.
11. Chen YS, Green CR, Danesh Meyer HV, Rupenthal ID. Neuroprotection in the treatment of glaucoma–A focus on connexin43 gap junction channel blockers. Eur J Pharm Biopharm. 2015.

https://doi.org/10.1016/j.ejpb.2015.01.031. ;95(Pt B :182 – 93.

12. Matsuda T, Fujio Y, Nariai T, Ito T, Yamane M, Takatani T, et al. N-cadherin signals through Rac1 determine the localization of connexin 43 in cardiac myocytes. J Mol Cell Cardiol. 2006;40(4):495–502. https://doi.org/10.1016/j.yjmcc.2005.12.010.
13. Adam O, Lavall D, Theobald K, Hohl M, Grube M, Ameling S, et al. Rac1-induced connective tissue growth factor regulates connexin 43 and N-cadherin expression in atrial fibrillation. J Am Coll Cardiol. 2010;55(5):469–80. https://doi.org/10.1016/j.jacc.2009.08.064.
14. Ram R, Wescott AP, Varandas K, Dirksen RT, Blaxall BC. Mena associates with Rac1 and modulates connexin 43 remodeling in cardiomyocytes. Am J Physiol Heart Circ Physiol. 2014;306(1):H154-9. https://doi.org/10.1152/ajpheart.00749.2013.
15. Kim HJ, Kim MJ, Mostafa MN, Park JH, Choi HS, Kim YS, et al. RhoA/ROCK regulates prion pathogenesis by controlling connexin 43 activity. Int J Mol Sci. 2020;21(4):1255. https://doi.org/10.3390/ijms21041255.
16. Zhang ML, Zhao GL, Hou Y, Zhong SM, Xu LJ, Li F, et al. Rac1 conditional deletion attenuates retinal ganglion cell apoptosis by accelerating autophagic flux in a mouse model of chronic ocular hypertension. Cell Death Dis. 2020;11(9):734. https://doi.org/10.1038/s41419-020-02951-7.
17. Li LZ, Yin N, Li XY, Miao Y, Cheng S, Li F, et al. Rac1 Modulates excitatory synaptic transmission in mouse retinal ganglion cells. Neurosci Bull. 2019;35(4):673–87. https://doi.org/10.1007/s12264-019-00353-0.
18. Miao Y, Dong LD, Chen J, Hu XC, Yang XL, Wang Z. Involvement of calpain/p35-p25/Cdk5/NMDAR signaling pathway in glutamate-induced neurotoxicity in cultured rat retinal neurons. PloS one. 2012;7(8):e42318. https://doi.org/10.1371/journal.pone.0042318.
19. Gao F, Li F, Miao Y, Xu LJ, Zhao Y, Qian L, et al. Involvement of the MEK-ERK/p38-CREB/c-fos signaling pathway in Kir channel inhibition-induced rat retinal Müller cell gliosis. Sci Rep. 2017;7(1):1480. https://doi.org/10.1038/s41598-017-01557-y.
20. Dong LD, Gao F, Wang XH, Miao Y, Wang SY, Li F, et al. GluA2 trafficking is involved in apoptosis of retinal ganglion cells induced by activation of EphB/EphrinB reverse signaling in a rat chronic ocular hypertension model. J Neurosci. 2015;35(13):5409–21. https://doi.org/10.1523/JNEUROSCI.4376-14.2015.
21. Chever O, Lee CY, Rouach N. Astroglial connexin43 hemichannels tune basal excitatory synaptic transmission. J Neurosci. 2014;34(34):11228–32. https://doi.org/10.1523/JNEUROSCI.0015-14.2014.
22. Slavi N, Toychiev AH, Kosmidis S, Ackert J, Bloomfield SA, Wulff H, et al. Suppression of connexin 43 phosphorylation promotes astrocyte survival and vascular regeneration in proliferative retinopathy. Proc Natl Acad Sci U S A. 2018;115(26):E5934-43. https://doi.org/10.1073/pnas.1803907115.
23. Ji Min, Miao Y, Dong LD, Chen J, Yang XL, Wang Z. Group I mGluR-mediated inhibition of Kir channels contributes to retinal Müller cell gliosis in a rat chronic ocular hypertension model. J Neurosci. 2012;32(37):12744–55. https://doi.org/10.1523/JNEUROSCI.1291-12.2012.

24. Peng W, Wu Z, Song K, Zhang S, Li Y, Xu M. Regulation of sleep homeostasis mediator adenosine by basal forebrain glutamatergic neurons. Science. 2020;369(6508):eabb0556. https://doi.org/10.1126/science.abb0556.
25. Liu T, Li Y, Zhang B, Ma L, Liu W, Li Z, et al. The role of phosphorylated Cx43 on PKC mediated Ser368 in lung injury induced by seawater inhalation. Inflammation. 2015;38(5):1847–54. https://doi.org/10.1007/s10753-015-0162-9.
26. Du ZJ, Cui GQ, Zhang J, Liu XM, Zhang ZH, Jia Q, et al. Inhibition of gap junction intercellular communication is involved in silica nanoparticles-induced H9c2 cardiomyocytes apoptosis via the mitochondrial pathway. Int J Nanomed. 2017;12:2179–88. https://doi.org/10.2147/IJN.S127904.
27. Li X, Jiang S, Yang H, Liao Q, Cao S, Yan X, et al. Breakthrough cancer pain is associated with spinal gap junction activation via regulation of connexin 43 in a mouse model. Front Cell Neurosci. 2017;11:207. https://doi.org/ 10.3389/fncel.2017.00207.
28. Xie Y, Liu S, Hu S, Wei Y. Cardiomyopathy-associated gene 1-sensitive PKC-dependent connexin 43 expression and phosphorylation in left ventricular noncompaction cardiomyopathy. Cell Physiol Biochem. 2017;44(2):828–42. https://doi.org/10.1159/000485348.
29. Yin X, Feng L, Ma D, Yin P, Wang X, Hou S, et al. Roles of astrocytic connexin-43, hemichannels, and gap junctions in oxygen-glucose deprivation/reperfusion injury induced neuroinflammation and the possible regulatory mechanisms of salvianolic acid B and carbenoxolone. J Neuroinflammation. 2018;15(1):97. https://doi.org/10.1186/s12974-018-1127-3.
30. Hung CC, Lin CH, Chang H, Wang CY, Lin SH, Hsu PC, et al. Astrocytic GAP43 induced by the TLR4/NF-κB/STAT3 axis attenuates astrogliosis-mediated microglial activation and neurotoxicity. J Neurosci. 2016;36(6):2027–43. https://doi.org/10.1523/JNEUROSCI.3457-15.2016.
31. Tedeschi A, Nguyen T, Puttagunta R, Gaub P, Di Giovanni S. A p53-CBP/p300 transcription module is required for GAP-43 expression, axon outgrowth, and regeneration. Cell Death Differ. 2009;16(4):543–54. https://doi.org/10.1038/cdd.2008.175.
32. Machesky LM, Hall A. Rho: a connection between membrane receptor signalling and the cytoskeleton. Trends Cell Biol. 1996;6(8):304 – 10. https://doi.org/10.1016/0962-8924(96)10026-x.
33. Machesky LM, Hall A. Role of actin polymerization and adhesion to extracellular matrix in Rac- and Rho-induced cytoskeletal reorganization. J Cell Biol. 1997;138(4):913–26. https://doi.org/10.1083/jcb.138.4.913.
34. Danesh Meyer HV, Zhang J, Acosta ML, Rupenthal ID, Green CR. Connexin43 in retinal injury and disease. Prog Retin Eye Res. 2016;51:41–68. https://doi.org/10.1016/j.preteyeres.2015.09.004.
35. Lin JHC, Lou N, Kang N, Takano T, Hu F, Han X, et al. A central role of connexin 43 in hypoxic preconditioning. J Neurosci. 2008;28(3):681–95. https://doi.org/10.1523/JNEUROSCI.3827-07.2008.
36. Mylvaganam S, Zhang L, Wu C, Zhang ZJ, Samoilova M, Eubanks J, et al. Hippocampal seizures alter the expression of the pannexin and connexin transcriptome. J Neurochem. 2010;112(1):92–102. https://doi.org/10.1111/j.1471-4159.2009.06431.x. Epub 2009 Oct 13.

37. Garbelli R, Frassoni C, Condorelli DF, Trovato Salinaro A, Musso N, Medici V, et al. Expression of connexin 43 in the human epileptic and drug-resistant cerebral cortex. Neurology. 2011;76(10):895–902. https://doi.org/10.1212/WNL.0b013e31820f2da6.
38. Dupont E, Matsushita T, Kaba RA, Vozzi C, Coppen SR, Khan N, et al. Altered connexin expression in human congestive heart failure. J Mol Cell Cardiol. 2001;33(2):359–71. https://doi.org/10.1006/jmcc.2000.1308.
39. Ai X, Pogwizd SM. Connexin 43 downregulation and dephosphorylation in nonischemic heart failure is associated with enhanced colocalized protein phosphatase type 2A. Circ Res. 2005;96(1):54–63. https://doi.org/10.1161/01.RES.0000152325.07495.5a.
40. Zhao M, Hou S, Feng L, Shen P, Nan D, Zhang Y, et al. Vinpocetine protects against cerebral ischemia-reperfusion injury by targeting astrocytic connexin43 via the PI3K/AKT signaling pathway. Front Neurosci. 2020;14:223. https://doi.org/10.3389/fnins.2020.00223.
41. Carlen PL. Curious and contradictory roles of glial connexins and pannexins in epilepsy. Brain Res. 2012;1487:54–60. https://doi.org/10.1016/j.brainres.2012.06.059.
42. Yoshioka J, Prince RN, Huang H, Perkins SB, Cruz FU, MacGillivray C, et al. Cardiomyocyte hypertrophy and degradation of connexin43 through spatially restricted autocrine/paracrine heparin-binding EGF. Proc Natl Acad Sci U S A. 2005;102(30):10622–7. https://doi.org/10.1073/pnas.0501198102.
43. Leithe E, Rivedal E. Epidermal growth factor regulates ubiquitination, internalization and proteasome-dependent degradation of connexin43. J Cell Sci. 2004;117(Pt 7):1211–20. https://doi.org/10.1242/jcs.00951.
44. Ueki T, Fujita M, Sato K, Asai K, Yamada K, Kato T. Epidermal growth factor down-regulates connexin-43 expression in cultured rat cortical astrocytes. Neurosci Lett. 2001;313(1–2):53–6. https://doi.org/10.1016/s0304-3940(01)02249-2.
45. Ribeiro Rodrigues TM, Martins Marques T, Morel S, Kwak BR, Girão H. Role of connexin 43 in different forms of intercellular communication - gap junctions, extracellular vesicles and tunnelling nanotubes. J Cell Sci. 2017;130(21):3619–30. https://doi.org/10.1242/jcs.200667.
46. Dunn CA, Lampe PD. Injury-triggered Akt phosphorylation of Cx43: a ZO-1-driven molecular switch that regulates gap junction size. J Cell Sci. 2014;127(Pt 2):455–64. https://doi.org/10.1242/jcs.142497.
47. Yogo K, Ogawa T, Akiyama M, Ishida-Kitagawa N, Sasada H, Sato E, et al. PKA implicated in the phosphorylation of Cx43 induced by stimulation with FSH in rat granulosa cells. J Reprod Dev. 2006;52(3):321–8. https://doi.org/10.1262/jrd.17107.
48. Li Y, Li D, Ying X, Khaw PT, Raisman G. An energy theory of glaucoma. Glia. 2015;63(9):1537–52. https://doi.org/10.1002/glia.22825.
49. Ai X, Jiang A, Ke Y, Solaro RJ, Pogwizd SM. Enhanced activation of p21-activated kinase 1 in heart failure contributes to dephosphorylation of connexin 43. Cardiovasc Res. 2011;92(1):106–14. https://doi.org/10.1093/cvr/cvr163.

50. DerMardirossian C, Schnelzer A, Bokoch GM. Phosphorylation of RhoGDI by Pak1 mediates dissociation of Rac GTPase. Mol Cell. 2004;15(1):117–27. https://doi.org/10.1016/j.molcel.2004.05.019.
51. Kobayashi K, Tsubosaka Y, Hori M, Narumiya S, Ozaki H, Murata T. Prostaglandin D2-DP signaling promotes endothelial barrier function via the cAMP/PKA/Tiam1/Rac1 pathway. Arterioscler Thromb Vasc Biol. 2013;33(3):565–71. https://doi.org/10.1161/ATVBAHA.112.300993.
52. Zhao L, Li AQ, Zhou TF, Zhang MQ, Qin XM. Exendin-4 alleviates angiotensin II-induced senescence in vascular smooth muscle cells by inhibiting Rac1 activation via a cAMP/PKA-dependent pathway. Am J Physiol Cell Physiol. 2014;307(12):C1130-41. https://doi.org/10.1152/ajpcell.00151.2014.
53. Kim MO, Ryu JM, Suh HN, Park SH, Oh YM, Lee SH, et al. cAMP promotes cell migration through cell junctional complex dynamics and actin cytoskeleton remodeling: implications in skin wound healing. Stem Cells Dev. 2015;24(21):2513–24. https://doi.org/10.1089/scd.2015.0130.
54. Darrow BJ, Laing JG, Lampe PD, Saffitz JE, Beyer EC. Expression of multiple connexins in cultured neonatal rat ventricular myocytes. Circ Res. 1995;76(3):381–7. https://doi.org/10.1161/01.res.76.3.381.
55. Paulson AF, Lampe PD, Meyer RA, TenBroek E, Atkinson MM, Walseth TF, et al. Cyclic AMP and LDL trigger a rapid enhancement in gap junction assembly through a stimulation of connexin trafficking. J Cell Sci. 2000;113(Pt 17):3037–49. https://doi.org/10.1007/BF00235042.
56. Shim MS, Kim KY, Bu JH, Nam HS, Jeong SW, Park TL, et al. Elevated intracellular cAMP exacerbates vulnerability to oxidative stress in optic nerve head astrocytes. Cell Death Dis. 2018;9(3):285. https://doi.org/10.1038/s41419-017-0171-8.
57. Beckel JM, Argall AJ, Lim JC, Xia J, Lu W, Coffey EE, et al. Mechanosensitive release of adenosine 5'-triphosphate through pannexin channels and mechanosensitive upregulation of pannexin channels in optic nerve head astrocytes: a mechanism for purinergic involvement in chronic strain. Glia. 2014;62(9):1486–501. https://doi.org/10.1002/glia.22695.
58. Zhu J, Li P, Zhou YG, Ye J. Altered energy metabolism during early optic nerve crush injury: implications of Warburg-like aerobic glycolysis in facilitating retinal ganglion cell survival. Neurosci Bull. 2020;36(7):761–77. https://doi.org/10.1007/s12264-020-00490-x.
59. Ishii T, Warabi E, Mann GE. Circadian control of p75 neurotrophin receptor leads to alternate activation of Nrf2 and c-Rel to reset energy metabolism in astrocytes via brain-derived neurotrophic factor. Free Radic Biol Med. 2018;119:34–44. https://doi.org/10.1016/j.freeradbiomed.2018.01.026.
60. Li Q, Qin T, Bi Z, Hong H, Ding L, Chen J, et al. Rac1 activates non-oxidative pentose phosphate pathway to induce chemoresistance of breast cancer. Nat commun. 2020;11(1):1456. https://doi.org/10.1038/s41467-020-15308-7.
61. Burnstock G. Physiology and pathophysiology of purinergic neurotransmission. Physiol Rev. 2007;87(2):659–797. https://doi.org/10.1152/physrev.00043.2006.
62. Abbracchio MP, Burnstock G, Verkhratsky A, Zimmermann H. Purinergic signalling in the nervous system: an overview. Trends Neurosci. 2009;32(1):19–29.

https://doi.org/10.1016/j.tins.2008.10.001.
63. Xue B, Xie Y, Xue Y, Hu N, Zhang G, Guan H, et al. Involvement of P2X receptors in retinal ganglion cell apoptosis induced by activated Müller cells. Exp Eye Res. 2016;153:42–50. https://doi.org/10.1016/j.exer.2016.10.005.
64. Newman EA. Glial cell inhibition of neurons by release of ATP. J Neurosci. 2003;23(5):1659–66. https://doi.org/10.1523/JNEUROSCI.23-05-01659.2003.
65. Boia R, Salinas Navarro M, Gallego Ortega A, Galindo Romero C, Aires ID, Agudo-Barriuso M, et al. Activation of adenosine A3 receptor protects retinal ganglion cells from degeneration induced by ocular hypertension. Cell Death Dis. 2020;11(5):401. https://doi.org/10.1038/s41419-020-2593-y.
66. Reichenbach A, Bringmann A. Purinergic signaling in retinal degeneration and regeneration. Neuropharmacology. 2016;104:194–211. https://doi.org/10.1016/j.neuropharm.2015.05.005.
67. Zhang X, Zhang M, Laties AM, Mitchell CH. Stimulation of P2X7 Receptors Elevates Ca2 + and Kills Retinal Ganglion Cells. Invest Ophthalmol Vis Sci. 2005;46(6):2183–91. https://doi.org/10.1167/iovs.05-0052.
68. Murphy Royal C, Johnston AD, Boyce AKJ, Diaz Castro B, Institoris A, Peringod G, et al. Stress gates an astrocytic energy reservoir to impair synaptic plasticity. Nat Commun. 2020;11(1):2014. https://doi.org/10.1038/s41467-020-15778-9.
69. Cooper ML, Pasini S, Lambert WS, D'Alessandro KB, Yao V, Risner ML, et al. Redistribution of metabolic resources through astrocyte networks mitigates neurodegenerative stress. Proc Natl Acad Sci U S A. 2020;117(31):18810–21. https://doi.org/10.1073/pnas.2009425117.

Figures

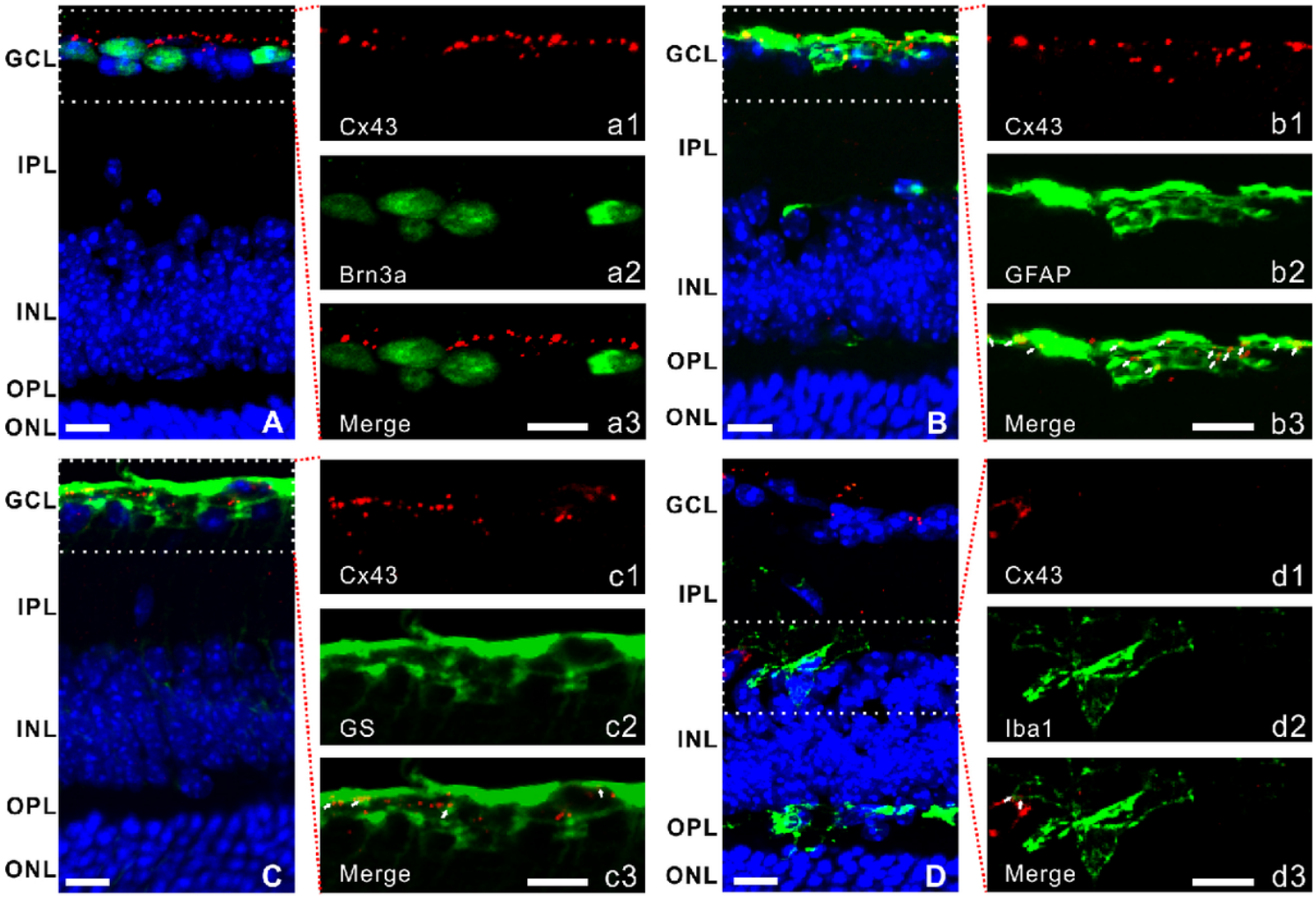

Fig. 1. Zhao et al.

Figure 1

Expression and distribution of Cx43 in mouse retina. (A-D) Double-immunofluorescence staining showing the co-localization of Cx43 with Brn3a, a marker of RGCs (A), GFAP, a marker of astrocytes (B), GS, a marker of Müller cells (C), or Iba1, a marker of microglial cells (D), in retinal vertical sections. a1-a3, b1-b3, c1-c3, and d1-d3 are the enlarged images of the white squares in A, B, C, and D, respectively. Scale bars: 10 μm. Arrows indicate double labeled immunofluorescent signals. Abbreviations: Brn3a, brain-specific homeobox/POU domain protein 3A; GFAP, glial fibrillary acidic protein; GS, glutamine synthetase; Iba1, ionized calcium binding adapter molecule 1; GCL: ganglion cell layer; IPL: inner plexiform layer; INL: inner nuclear layer, OPL: outer plexiform layer; ONL: outer nuclear layer.

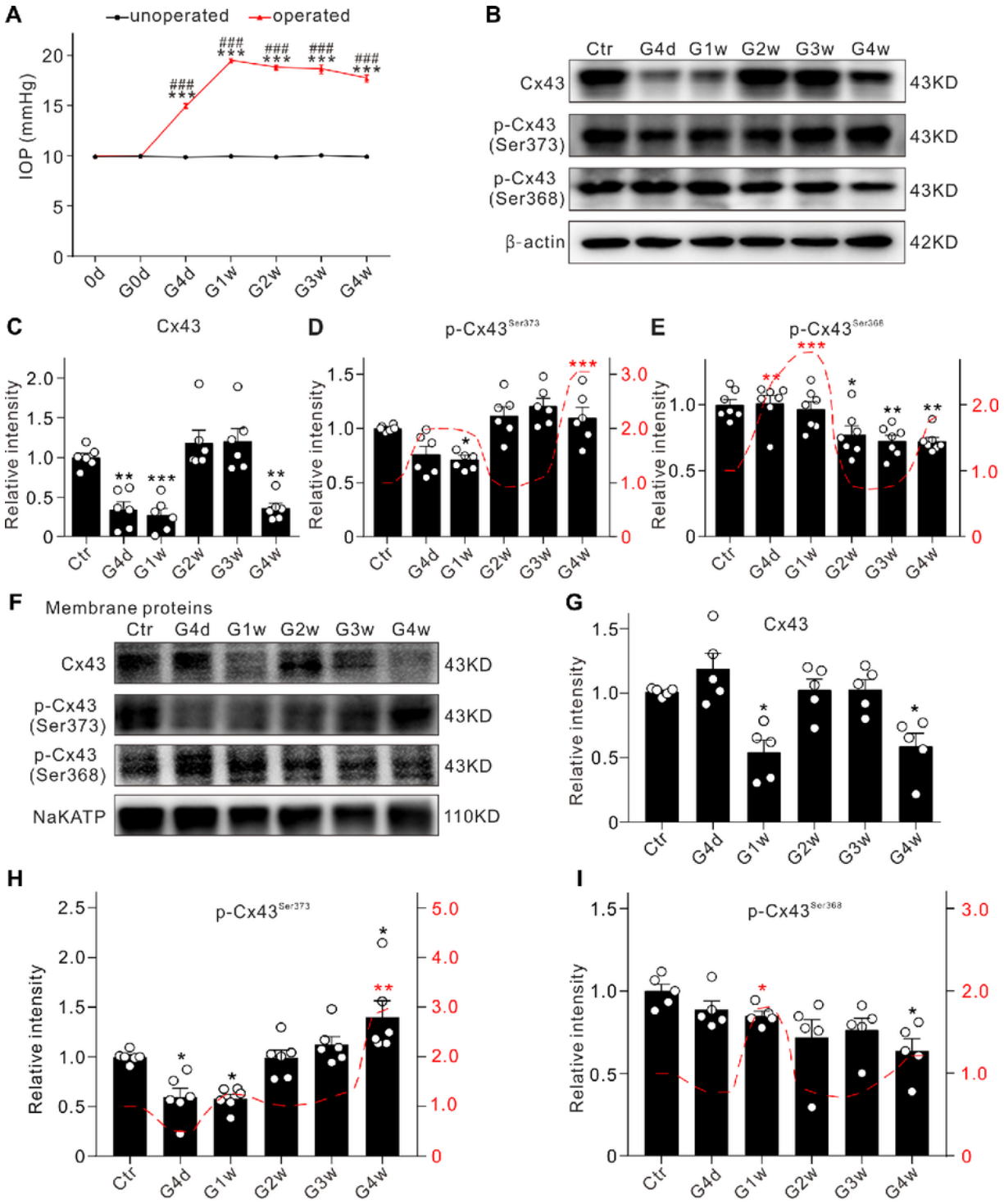

Fig. 2. Zhao et al.

Figure 2

Changes in protein levels of Cx43 and phosphorylated Cx43 in COH retinas. (A) Changes of IOP in both eyes of COH mice. ***P < 0.001 vs. 0d, and ###P < 0.001 vs. unoperated eyes (left eyes) at the same time point. (B-E) Representative immunoblots obtained at different times after the operation showing the changes of Cx43, p-Cx43ser373, and p-Cx43ser368 protein levels (B). Average relative densities of immunoreactive bands of these proteins are shown in C-E, respectively. All data are normalized to their

corresponding β-actin and then to the controls (Ctr). Red dash lines indicate the ratios of p-Cx43Ser373/Cx43 (D) and p-Cx43Ser368/Cx43 (E). (F-I) Representative immunoblots obtained at different times after the operation showing the changes of Cx43, p-Cx43ser373, and p-Cx43ser368 protein levels in cell membrane component (F). Average relative densities of immunoreactive bands of these proteins are shown in G-I, respectively. All data are normalized to their corresponding NaKATP and then to Ctr. Red dash lines indicate the ratios of p-Cx43Ser373/Cx43 (H) and p-Cx43Ser368/Cx43 (I). n = 5~7. *P < 0.05, **P < 0.01, and ***P < 0.001 vs. Ctr. One-way ANOVA with Tukey's multiple comparison test.

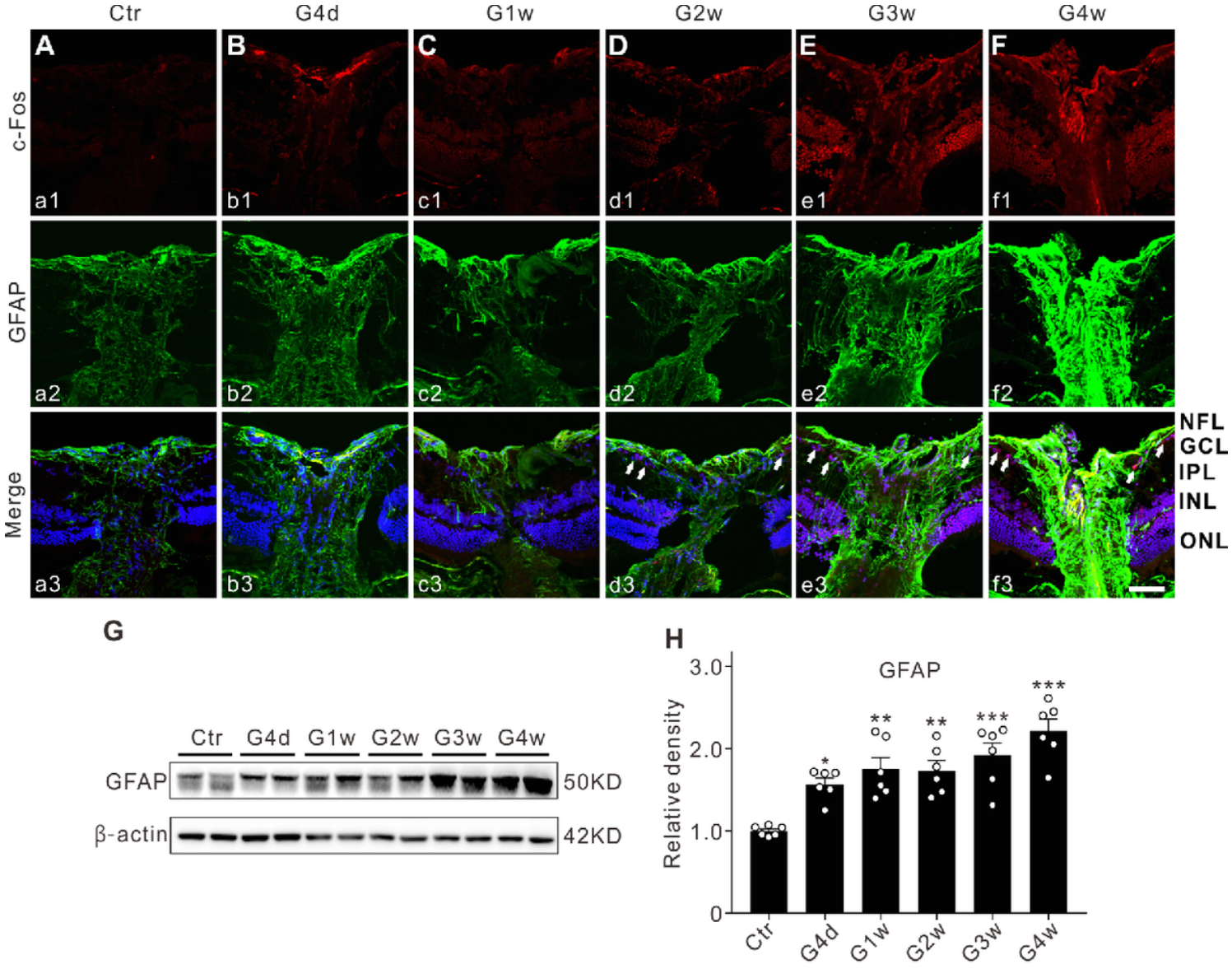

Fig. 3. Zhao et al.

Figure 3

The activation of astrocytes in the COH retinas. (A-F) Double-immunofluorescence staining showing c-Fos (red) and GFAP (green) expression in mice retinal vertical slices taken from the ONH of sham-operated retina (Ctr) (A), and those obtained at different post-operational times (G4d, G1w, G2w, G3w, and G4w) (B-F). Scale bar: 50 μm for all images. Arrows indicate c-Fos expression in RGCs. (G, H)

Representative immunoblots obtained at different times after the operation showing the changes of GFAP expression (G). Average relative densities of immunoreactive bands of GFAP are shown in H. All data are normalized to their corresponding β-actin data and then to Ctr. n = 6 for each group. *P < 0.05, **P < 0.01, and ***P < 0.001 vs. Ctr. One-way ANOVA with Tukey's multiple comparison test.

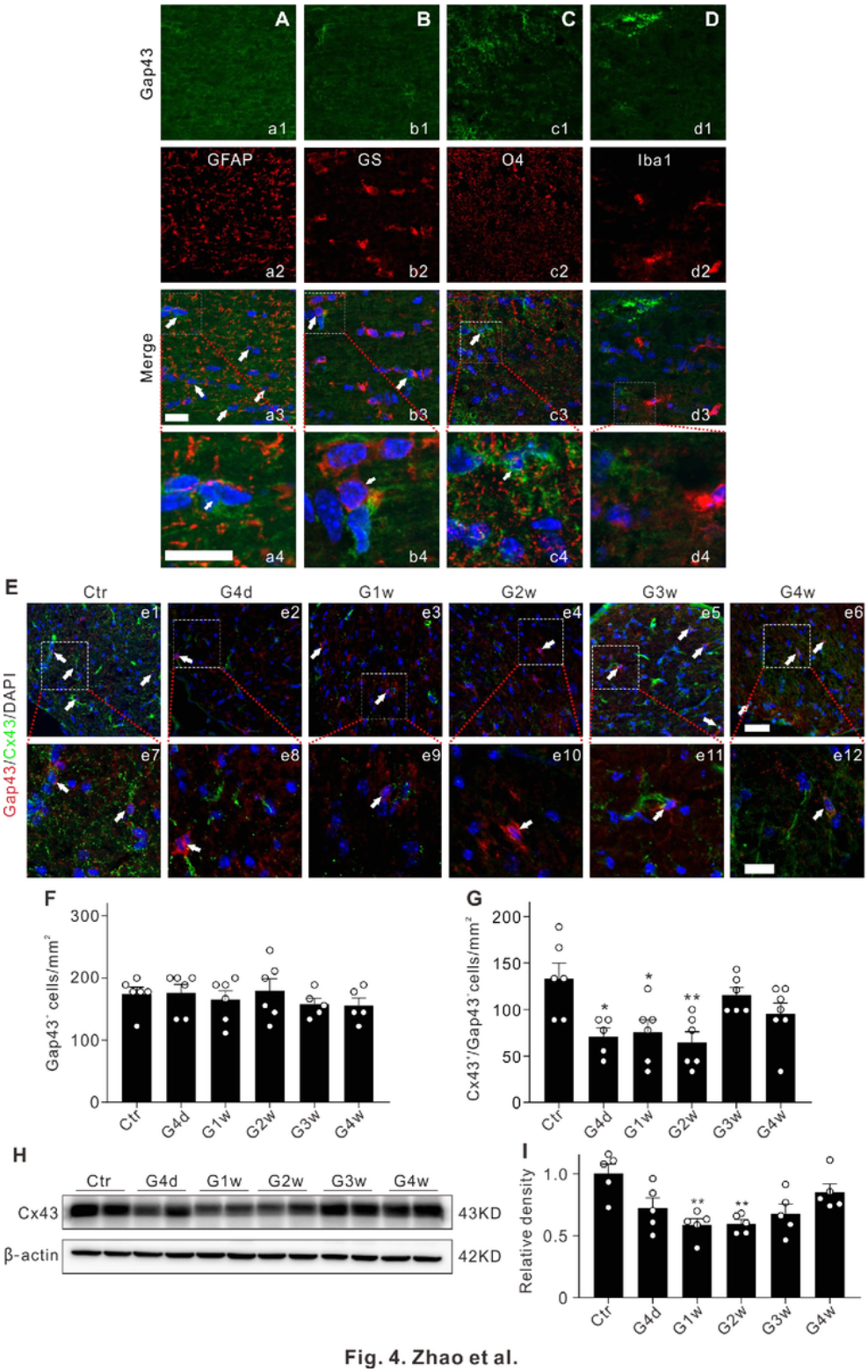

Fig. 4. Zhao et al.

Figure 4

Change of astrocyte plasticity may lead to decrease of Cx43 expression in the ONH of COH mice. (A-D) Micrographs showing double-immunostaining of Gap43 expression in astrocytes labeled by GFAP (A, a1-a3), Müller cells labeled by GS (B, b1-b3), oligodendrocytes labeled by O4 (C, c1-c3), microglia labeled by Iba1 (D, d1-d3) in the ONH of mice. a4-d4 are the enlarged images of the white squares of a3-d3, respectively. Scale bars: 10 μm. (E) Micrographs showing double-immunostaining of co-localization of Gap43 and Cx43 in the ONH taken from control (Ctr) mice (e1) and those at different post-operational times (G4d-G4w) (e2-e6). Scale bars: 20 μm. e7-e12 are the enlarged images of the white squares of e1-e6, respectively. Scale bar: 10 μm. (F) Bar charts showing the average number of Gap43 labeled cells/mm2 in the ONH of mice under different conditions as shown in E. (G) Bar charts showing the average number of Gap43 and Cx43 double-labeled cells/mm2 in the ONH of mice under different conditions as shown in E. n = 5~7. *P < 0.05 and **P < 0.01 vs. Ctr. (H, I) Representative immunoblots (H) and the densitometric quantification (I) showing the changes of Cx43 protein expression in the ONH of control (Ctr) mice and COH mice at different post-operational times (G4d-G4w). All data are normalized to their corresponding β-actin and then to Ctr. n = 5. **P < 0.01 vs. Ctr. One-way ANOVA with Tukey's multiple comparison test. Abbreviations: GFAP, glial fibrillary acidic protein; GS, glutamine synthetase; O4, an antigen on the surface of oligodendrocyte progenitors; Iba1, Ionized calcium binding adapter molecule 1; Gap43, growth-associated protein 43.

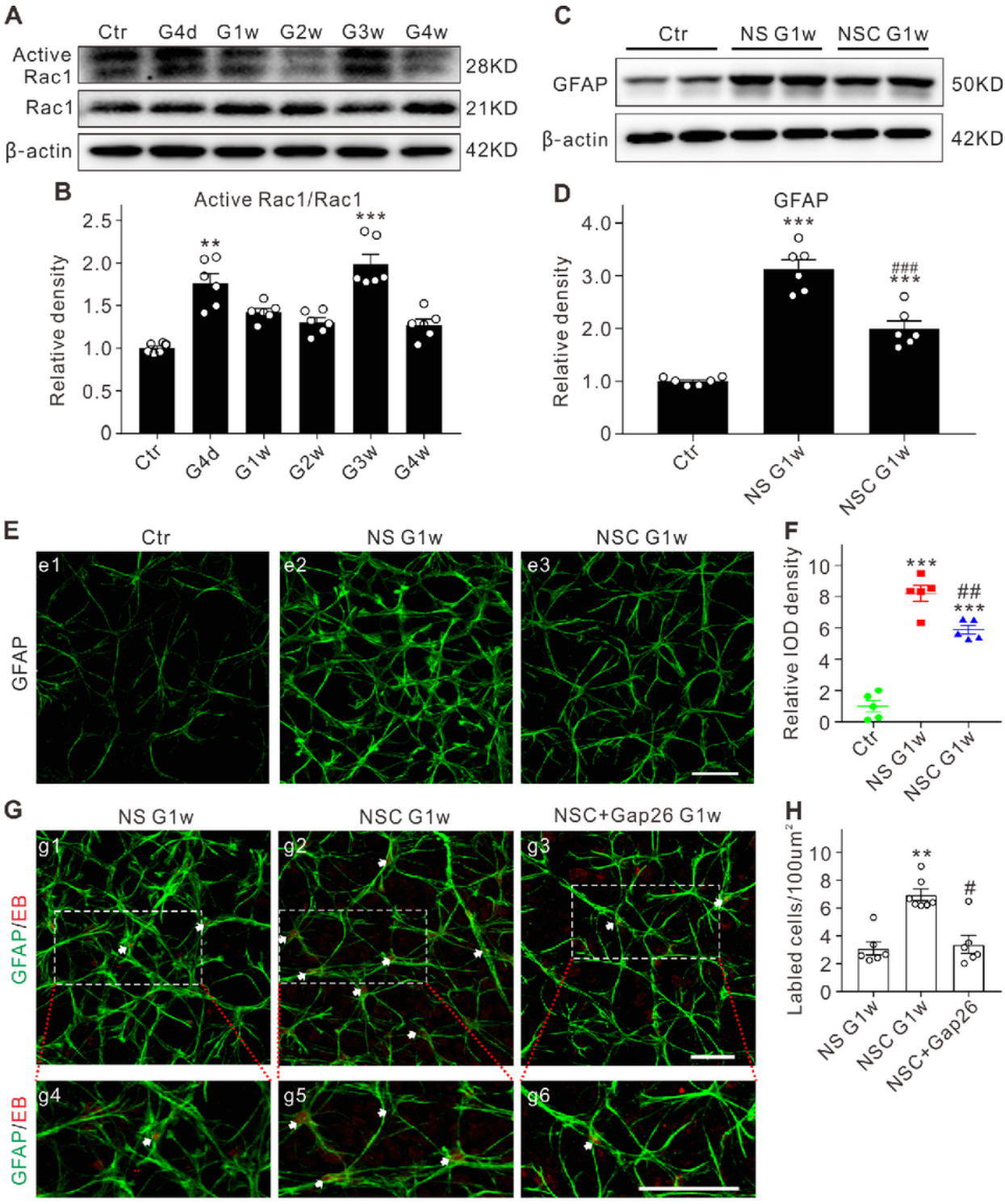

Fig. 5. Zhao et al.

Figure 5

Rac1 regulates astrocyte activity and Cx43 hemichannel permeation. (A, B) Representative immunoblots (A) and the densitometric quantification (B) showing the changes of active Rac1 and Rac1 expression levels in retinal homogenates of control (Ctr) mice and COH mice at different post-operational times (G4d-G4w). (C, D) Representative immunoblots (C) and the densitometric quantification (D) showing the changes of GFAP levels in retinas of control (Ctr) mice, and COH mice at G1w with normal saline (NS) (NS

G1w) or NSC23766 (NSC G1w) injections. All data are normalized to their corresponding β-actin and then to Ctr. n = 6 for all the groups. **P < 0.01, ***P < 0.001 vs. Ctr. ###P < 0.001 vs. NS G1w. One-way ANOVA with Tukey's multiple comparison test. (E) Representative images showing the GFAP immunofluorescence, taken from whole flat-mounted retinas of Ctr (e1), NS G1w (e2) and NSC23766 G1w (e3) groups. Scale bar: 50 μm. (F) Bar charts summarizing the relative integrated optical density (IOD) of GFAP immunofluorescence under different conditions as shown in E. Eight regions in each retina were selected from both central and peripheral regions for analysis. n = 5 for all the groups. ***P < 0.001 vs. Ctr. ##P < 0.01 vs. NS G1w. (G) Representative images showing the hemichannel activity as measured by ethidium bromide (EtBr) uptake (red) in astrocytes, taken from whole flat-mounted retinas of COH mice at G1w with NS (NS G1w) (g1), NSC23766 (NSC G1w) (g2) and NSC23766+Gap26 (NSC+Gap26 G1w) (g3) injections. g4-g6 are the enlarged images of the white squares in g1, g2, and g3, respectively. Scale bar: 50 μm. (H) Bar charts summarizing the changes in average number of the labeled cells of EtBr uptake in astrocytes under different conditions as shown in G. Eight regions in each retina were selected from both central and peripheral regions for analysis. n = 6~7. **P < 0.01 vs. NS G1w. #P < 0.05 vs. NSC G1w. One-way ANOVA with Tukey's multiple comparison test.

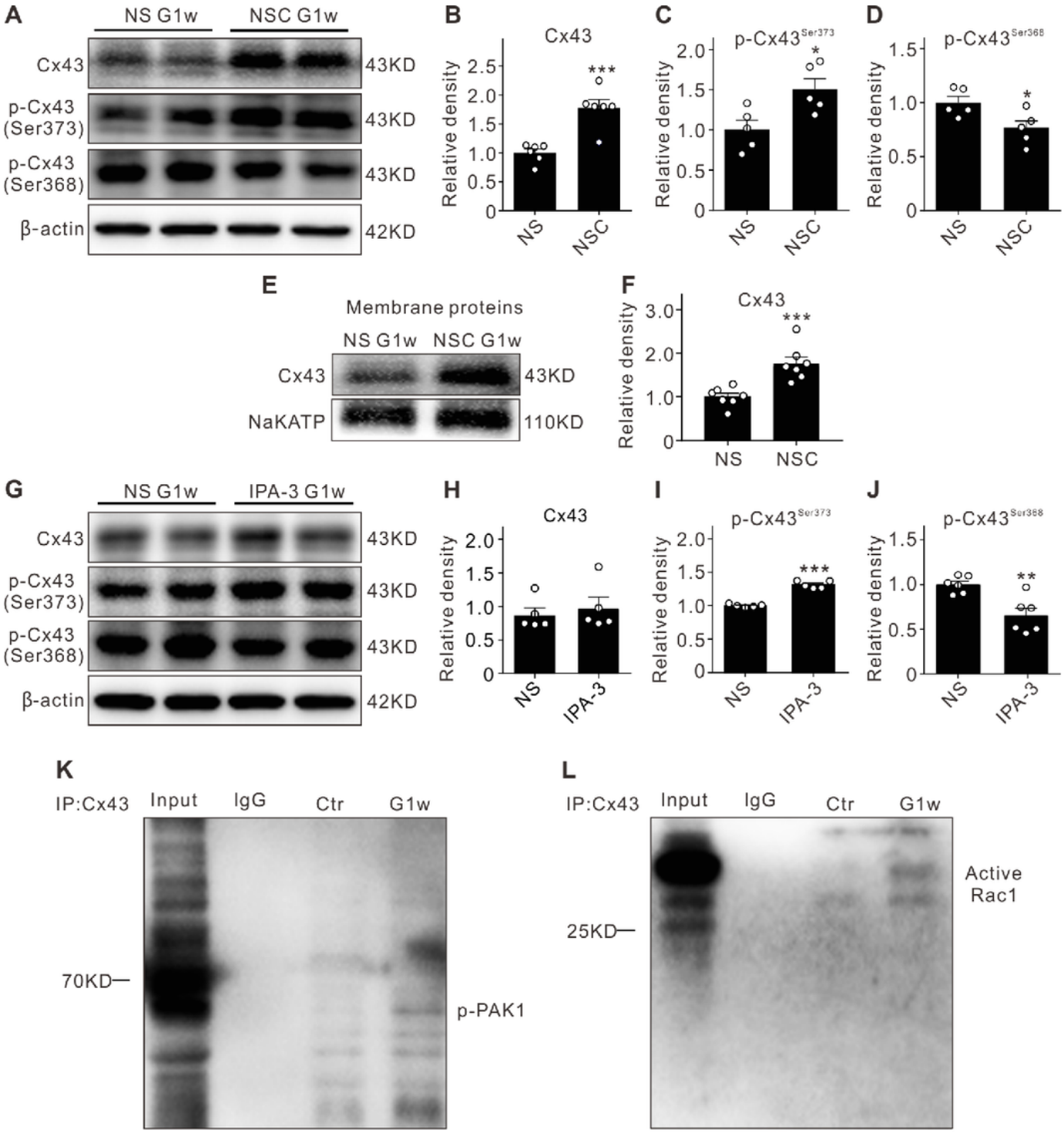

Fig. 6. Zhao et al.

Figure 6

Rac1 regulates Cx43 expression through Pak1. (A-D) Representative immunoblots (A) and the densitometric quantification (B-D) showing the changes of Cx43, p-Cx43Ser373, p-Cx43Ser368 levels in COH retinas at G1w with normal saline (NS) and NSC23766 (NSC) injections. (E, F) Representative immunoblots (E) and the densitometric quantification (F) showing the changes of Cx43 levels in membrane component of COH retinas at G1w with NS and NSC23766 (NSC) injections. (G-J)

Representative immunoblots (G) and the densitometric quantification showing the changes of Cx43 (H), p-Cx43Ser373 (I), and p-Cx43Ser368 (J) in COH retinas with NS and IPA-3 injections. Data are first normalized to their corresponding β-actin (or NaKATP) and then to NS. n = 5~7. *P < 0.05, **P < 0.01, and ***P < 0.001 vs. NS. Two-tailed unpaired t-test. (K, L) Co-IP experiments showing the interactions of Cx43 with p-PAK1 (K) or active Rac1 (L) in retinas of Ctr and COH at G1w. Bands of p-PAK1 at the location corresponding to 61 kDa were detected using the antibody against Cx43. Bands of active Rac1 at the location corresponding to 28 kDa were detected using the antibody against Cx43.

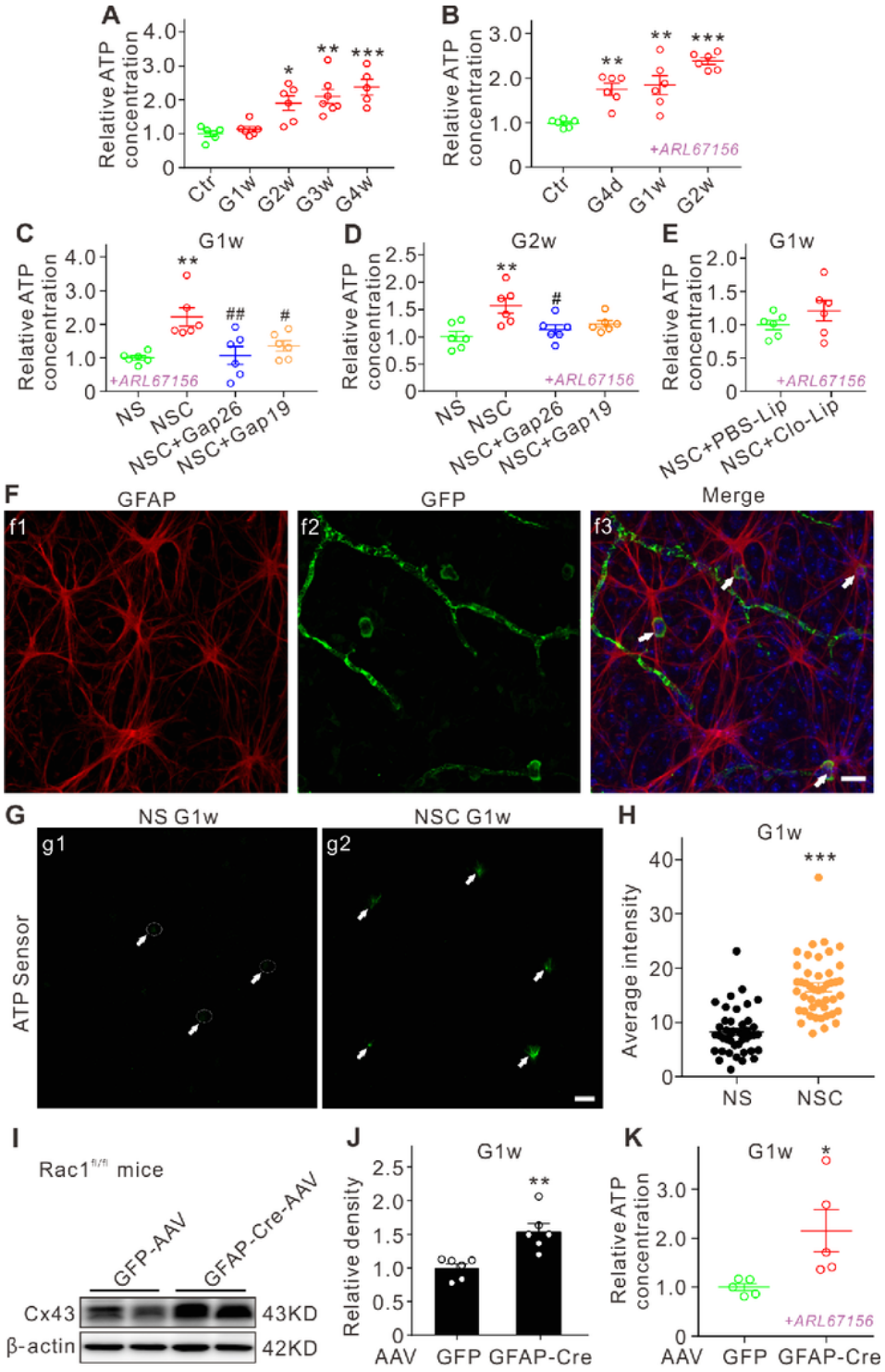

Fig. 7. Zhao et al.

Figure 7

Inhibiting Rac1 or conditional knockout of Rac1 in astrocytes increases ATP release. (A, B) Changes in ATP levels assayed by luciferin-luciferase method in retinas of control (Ctr) and COH mice at different post-operational times without (A) or with (B) the addition of the ecto-ATPase inhibitor ARL67156. All data are normalized to Ctr. n = 5~7. *P < 0.05, **P < 0.01, and ***P < 0.001 vs. Ctr. One-way ANOVA with Tukey's multiple comparison test. (C, D) Changes in ATP levels in COH retinas at G1w (C) or G2w (D) with normal saline (NS), NSC23766 (NSC), NSC23766+Gap26 (NSC+Gap26), and NSC23766+Gap19 (NSC+Gap19) injections, respectively. All data are normalized to NS groups. n = 6 for all the groups. **P < 0.01 vs. NS; #P < 0.05 and ## P <0.01 vs. NSC. One-way ANOVA with Tukey's multiple comparison test. (E) Changes in the ATP levels in COH retinas with or without microglia deletion by clodronate liposomes (Clo-Lip) at G1w. n = 6. Two-tailed unpaired t-test. (F) Representative images of immunostaining for GFAP and GFP (labeled ATP sensor), taken from whole flat-mounted retina with injections of AAV2-EFS-DIO-ATP1.0 probe in the hGFAP-Cre mice. Scale bar: 20 μm. Arrows indicate the double immunofluorescent labeling of GFAP and GFP in astrocytes. (G, H) Representative images (G) and the average intensity of GFP fluorescence signals (H) in COH retinas at G1w with NS (g1) or NSC (g2) injections, taken from whole flat-mounted retinas with injections of AAV2-EFS-DIO-ATP1.0 probe in the hGFAP-Cre mice. Scale bar: 30 μm. Arrows indicate the increased ATP fluorescence signals (green). n = 43~45 cells of 3 mice. ***P < 0.001 vs. NS. (I, J) Representative immunoblots (I) and the densitometric quantification (J) showing the changes of Cx43 in COH retinas with sub-retinal injections of GFP-AAV or GFAP-Cre-AAV in Rac1$^{fl/fl}$ mice. All data are normalized to GFP-AAV G1w. n = 6 for each group. **P < 0.01 vs. GFP-AAV G1w. (K) Bar charts showing the average ATP levels in GFP-AAV G1w, GFAP-Cre-AAV G1w retinas of Rac1$^{fl/fl}$ mice. All data are normalized to GFP group. n = 5 for each group. *P < 0.05 vs. GFP-AAV G1w. Two-tailed unpaired t-test.

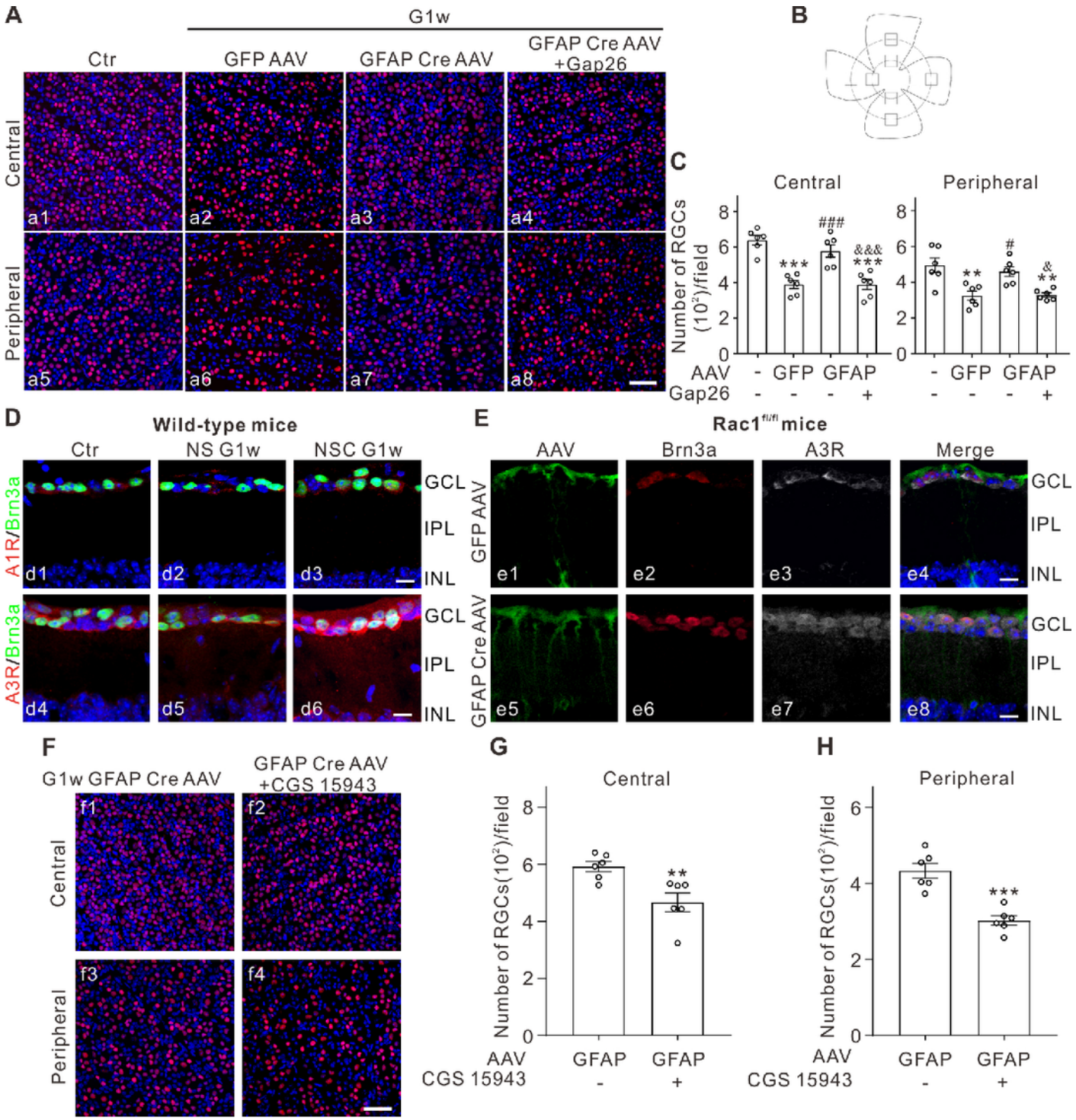

Fig. 8. Zhao et al.

Figure 8

Conditional knockout of Rac1 in astrocytes increases RGC survival through regulating adenosine receptors in COH retinas. (A) Typical micrographs of Brn3a-positive RGCs captured from normal (Ctr) and COH whole flat-mounted retinas at the same angle (0°) at G1w with injections of GFP-AAV, GFAP-Cre-AAV, and GFAP-Cre-AAV+Gap26 in Rac1fl/fl mice, respectively. Images are taken from central (a1-a4) and peripheral (a5-a8) regions. Scale bar: 50 μm for all images. (B) Diagrammatic sketch displaying the 8

chose fields for evaluating RGC survival. (C) Quantification of Brn3a-positive RGCs under different conditions as shown in A. n = 6 retinas for each group. **P < 0.01 and ***P < 0.001 vs. Ctr; #P < 0.05 and ###P < 0.001 vs. GFP-AAV G1w; &P < 0.05 and &&&P < 0.001 vs. GFAP-Cre-AAV G1w. One-way ANOVA with Tukey's multiple comparison test. (D) Double immunofluorescence staining showing the changes of A1R (d1-d3) and A3R (d4-d6) expression in Brn3a-positive RGCs in retinal vertical slices taken from Ctr mice and COH mice at G1w with NS and NSC23766 injections, respectively. Scale bars: 10 μm. (E) Triple immunofluorescence staining showing the changes of A3R expression in Brn3a-positive RGCs in retinal vertical slices taken from COH retinas at G1w with injections of GFP-AAV (e1-e4) and GFAP-Cre-AAV (e5-e8) in Rac1$^{fl/fl}$ mice. Scale bars: 10 μm. (F) Typical micrographs of Brn3a-positive RGCs captured from COH whole flat-mounted retinas at the same angle (0°) at G1w with injections of GFAP-Cre-AAV and GFAP-Cre-AAV+CGS15943 in Rac1$^{fl/fl}$ mice, respectively. Scale bar: 50 μm. (G, H) Quantification of Brn3a-positive RGCs under different conditions as shown in F. n = 6 retinas for each group. **P < 0.01 and ***P < 0.001 vs. GFAP-Cre-AAV G1w. Two-tailed unpaired t-test.

Supplementary Files

This is a list of supplementary files associated with this preprint. Click to download.

- FigureS1.pdf
- FigureS2.pdf
- FigureS3.pdf
- SupplementaryFigureLegendsS1S3.docx
- SupplimentaryTable1antibodyusedintheexperiments.docx